PB-239 467

INFRARED GAS FILTER CORRELATION INSTRUMENT FOR IN-SITU MEASUREMENT OF GASEOUS POLLUTANTS

E. E. Burch, et al

Philco-Ford Corporation

Prepared for:

National Environmental Research Center

December 1974

DISTRIBUTED BY:

NTIS

National Technical Information Service
U. S. DEPARTMENT OF COMMERCE

BIBLIOGRAPHIC DATA SHEET	1. Report No. EPA-650/2-74-094	2.	PB 239 467

4. Title and Subtitle
Infrared Gas Filter Correlation Instrument for in situ Measurements of Gaseous Pollutants

5. Report Date
December 1974

6.

7. Author(s)
D. E. Burch and D. A. Gryvnak

8. Performing Organization Rept. No. U6121

9. Performing Organization Name and Address
Philco-Ford Corporation, Aeronutronic Division
Ford Road
Newport Beach, California 92663

10. Project/Task/Work Unit No.
1AA010/26AAP/14

11. Contract/Grant No.
EPA 68-02-0575

12. Sponsoring Organization Name and Address
Chemistry and Physics Laboratory
National Environmental Research Center
Environmental Protection Agency
Research Triangle Park, N. C. 27711

13. Type of Report & Period Covered Final Report
7/72 to 6/74

14.

15. Supplementary Notes

16. Abstracts An infrared analyzer employing gas cell correlation techniques has been designed and constructed to measure the concentrations of carbon monoxide, nitric oxide, sulfur dioxide, hydrogen chloride, and hydrogen fluoride in the effluent of stationary sources. An infrared beam is directed across the stack to a retroreflector and back so that the instantaneous average concentration is measured continuously without disturbing the constituents of the effluent. A small, removable, fixed-position grating monochromator acts as a unique optical filter that passes narrow spectral intervals that are centered at wavelengths where the gas to be detected will absorb. One grating monochromator is used for CO and NO, another for SO_2 and HCl, and a third for HF. The useful ranges of concentration times path length, in atm cm, over which each gas can be measured are: 0.005 to 0.4 to NO; 0.0013 to 0.15 for CO; 0.001 to 4.0 for SO_2; 0.0003 to 0.2 for HCl and 0.0001 to 0.02 for HF. The discrimination against other gases in the effluent is excellent. This report was submitted in fulfillment of contract number 68-02-0575 by Philco-Ford Corp., Aeronutronic Div., under the sponsorship of the Environmental Protection Agency.

17. Key Words and Document Analysis. 17a. Descriptors

Exhaust Gases
NO, CO, SO_2, HCl and HF
Infrared Analysis
Correlation Techniques

17b. Identifiers/Open-Ended Terms

Gaseous Pollutants
Gas Filter Correlation
Effluent Concentration
Stationary Source

17c. COSATI Field/Group

Reproduced by
NATIONAL TECHNICAL INFORMATION SERVICE
U S Department of Commerce
Springfield VA 22151

PRICES SUBJECT TO CHANGE

18. Availability Statement	19. Security Class (This Report)	21. No. of Pages
Release Unlimited	UNCLASSIFIED	64
	20. Security Class (This Page) UNCLASSIFIED	22. Price $4.25-2.25

APTIC #75058

EPA-650/2-74-094

INFRARED GAS FILTER CORRELATION INSTRUMENT FOR IN-SITU MEASUREMENT OF GASEOUS POLLUTANTS

by

D. E. Burch and D. A. Gryvnak

Philco-Ford Corporation
Newport Beach, CA 92663

Contract No. 68-02-0575
Program Element No. 1AA010
ROAP No. 26AAP

Project Officer: William F. Herget

Chemistry and Physics Laboratory
National Environmental Research Center
Research Triangle Park, North Carolina 27711

Prepared for

OFFICE OF RESEARCH AND DEVELOPMENT
ENVIRONMENTAL PROTECTION AGENCY
WASHINGTON, D.C. 20460

December 1974

This report has been reviewed by the Environmental Protection Agency and approved for publication. Approval does not signify that the contents necessarily reflect the views and policies of the Agency, nor does mention of trade names or commercial products constitute endorsement or recommendation for use.

ABSTRACT

An infrared analyzer employing gas cell correlation techniques has been designed and constructed to measure the concentrations of carbon monoxide, nitric oxide, sulfur dioxide, hydrogen chloride, and hydrogen fluoride in the effluent of stationary sources. An infrared beam is directed across the stack to a retroreflector and back so that the instantaneous average concentration is measured continuously without disturbing the constituents of the effluent. A small, removable, fixed-position grating monochromator acts as a unique optical filter that passes narrow spectral intervals that are centered at wavelengths where the gas to be detected will absorb. One grating monochromator is used for CO and NO, another for SO_2 and HCl, and a third for HF. The useful ranges of concentration times path length, in atm cm, over which each gas can be measured are: 0.005 to 0.4 to NO; 0.0013 to 0.15 for CO; 0.001 to 4.0 for SO_2; 0.0003 to 0.2 for HCl and 0.0001 to 0.02 for HF. The discrimination against other gases in the effluent is excellent.

This report was submitted in fulfillment of contract number 68-02-0575 by Philco-Ford Corporation, Aeronutronic Division, under the sponsorship of the Environmental Protection Agency.

CONTENTS

		PAGE
ABSTRACT		iii
ILLUSTRATIONS		v
LIST OF TABLES		vii
ACKNOWLEDGEMENT		viii
SECTION		
1	INTRODUCTION AND SUMMARY	1
	Background	1
	Brief Description of Instrument	2
	Definitions, Symbols and Units	3
2	SPECTROSCOPIC PRINCIPLES	5
	Correlation in Simple Spectral Models	5
	Energy and Voltage Relationships	11
	Design Factors	18
	Two-Cell System	20
	Multiple Correlation Cell Systems	24
3	INSTRUMENT DESIGN AND PERFORMANCE	25
	Optical Layout of Basic Instrument	25
	Instrument Employing Grating Assembly	29
	Spectral Properties of the Gases	35
	Laboratory Tests and Calibration Data	40
	Field Tests	47
4	REFERENCES	53

ILLUSTRATIONS

FIGURE		PAGE
1	Simplified optical diagram of a basic gas-cell correlation spectrometer.	6
2	Plots of transmittance for a model gas illustrating the spectroscopic principles of detection.	8
3	Plots of transmittance illustrating interference by a gas species other than the one being measured.	9
4	Plots of transmittance illustrating the effect of an absorbing gas of species y whose spectrum is not correlated with that of species x.	10
5	Simplified diagram of a gas-cell correlation spectrometer that employs high-frequency chopping and low-frequency modulation.	12
6	Calculated spectral plots of transmittance for a model spectrum similar to a portion of a CO band.	14
7	Plots of calculated $\overline{T_L \cdot T_{sam}}$ and $\overline{T_{att} \cdot T_{sam}}$ versus sample absorber thickness.	16
8	Plot of calculated Δ/Σ versus sample absorber thickness.	17
9	Calculated spectral plots of transmittance for a model spectrum illustrating the principle of detection of the two-cell system.	21
10	Calculated spectral plots of transmittance demonstrating the principles of discrimination against continuum absorption by the two-cell and the one-cell attenuator systems.	22
11	Optical diagram of a gas-cell correlation instrument for across-the-stack measurements.	26

ILLUSTRATIONS (continued)

FIGURE		PAGE
12	Optical diagram of a retroreflector assembly used to redirect the radiant energy beam back across the stack to the gas-cell correlation instrument.	28
13	Optical diagram of a gas-cell correlation instrument incorporating a grating assembly.	30
14	Optical diagram of a retroreflector and grid assembly.	32
15	The grating assembly for SO_2 and HCl.	33
16	The power supply unit above the electronics unit.	34
17	Photographs of the optical assembly.	36
18	Spectral curves of transmittance of H_2O and of H_2O + NO between 1862 and 1928 cm^{-1}.	37
19	Spectral curves of transmittance between 2465 and 2525 cm^{-1}.	39
20	Curves of V' versus normalized absorber thickness for CO and NO.	41
21	Curves of V' vs normalized absorber thicknesss for SO_2 and HCl.	42
22	Curve of V' vs normalized absorber thickness for HF.	43
23	The optics assembly and the retroreflector mounted on the smokestack of the Duke Power Co. at Charlotte, N. C.	48
24	Plots of NO concentration vs time for 3 different days at the Duke Power Co., Charlotte, N. C.	49
25	Plot of CO concentration vs time of day for 25 June 1974 at Duke Power Co., Charlotte, N. C.	50
26	Plots of SO_2 concentration vs time of day for 3 different days at Duke Power Co. In Charlotte, N. C.	52

LIST OF TABLES

TABLE		PAGE
1	Comparison of the sensitivity and discrimination of two-cell and one cell-attenuator system.	24
2	Instrument parameters and performance.	46

ACKNOWLEDGEMENT

The authors would like to express their gratitude to two of their co-workers, Mr. Francis J. Gates and Mr. John D. Pembrook, for their cooperation and assistance. Mr. Gates' ingenuity and skills in setting up test apparatus and in assembling small components were invaluable. Mr. Pembrook is responsible for designing and testing the electronic components.

SECTION 1

INTRODUCTION AND SUMMARY

BACKGROUND

Most commercially available instruments for measuring the concentrations of gaseous pollutants in the effluent of stationary sources require that a sample be drawn from a stack or duct through a probe into a separate container for analysis. The analysis may be made continuously on-line or at a later time, possibly in a laboratory. Such sampling techniques have two major drawbacks: (1) concentration changes may occur along the sampling train; and (2) concentration gradients may exist in the flow field so that several samples may need to be taken from different positions in order to determine the average concentration. By employing in-situ absorption spectroscopy, the first difficulty can be eliminated and the second one greatly reduced. In absorption spectroscopy radiant energy from a thermal source is transmitted through the effluent from one side of the duct to the other side. By comparing the amount of transmitted energy at characteristic wavelengths where a particular gas species absorbs strongly to that at wavelengths where it does not absorb, or absorbs weakly, it is possible to determine the instantaneous average concentration across the flow field. The effluent flow is undisturbed, and the measurement along the path across the duct adequately represents the average unless there are unusually large gradients in the concentration. The required wavelength selection for absorption spectroscopy may be achieved in a variety of ways. Narrow band interference filters provide a simple, relatively inexpensive method, but in most cases they do not provide the high spectral resolution required for good specificity, or discrimination against other gas species that may absorb in the same spectral interval. Dispersing instruments employing a prism or grating and a scanning mechanism provide better spectral resolution, but are more complex and, in turn, more expensive and more subject to misalignment.

A class of instruments employing gas-cell correlation spectroscopy to provide good sensitivity and specificity at relatively low cost have been developed for a variety of applications. Gas-cell correlation instruments of various types have been discussed in References 1-5. In one form, the energy beam transversing the sample gas is alternately directed through either a correlation cell or an attenuator. The correlation cell, also

frequently called a gas filter, contains the gas species to be measured, and the attenuator has nearly constant transmittance at all wavelengths of interest. An interference filter restricts the spectral bandpass to a region of absorption by the gas species being measured. The gas in the correlation cell is essentially opaque at the wavelengths of maximum absorption for the gas species being measured. Therefore, as the correlation cell and the attenuator are alternated in and out of the beam, the energy of wavelengths of strong absorption by the gas are modulated. In the following section, some very simple models of absorption spectra are used to describe the spectroscopic principles of detection and discrimination of gas-cell correlation spectrometers. The illustrations used are helpful in understanding many of the factors involved in designing a gas-cell correlation instrument for a particular application.

BRIEF DESCRIPTION OF INSTRUMENT

The primary purpose of the work reported here has been to perform the required research and to design and construct a gas-cell correlation instrument for across-the-stack monitoring of stationary source emissions. Any of the five gases, NO, CO, SO_2, HF, or HCl, can be measured over the concentration ranges ordinarily of interest for stationary sources. SO_2 was originally included, but subsequent research indicated that this gas could probably be measured better by methods other than gas-cell correlation spectroscopy.

Conversion of the instrument from one gas species to another is relatively simple and involves changing a correlation cell and a bandpass filter. Changing the radiant energy source and/or the detector may also be required, depending on the gas species involved. The instrument has been designed for versatility, it is necessarily more complex than an instrument designed to use the same principle of operation for a single gas species on a particular type of stack. In some cases, the stability, the signal-to-noise ratio and the ease of operation have been compromised in order to retain the versatility. The instrument is intended primarily as a tool for the Environmental Protection Agency to evaluate gas-cell correlation methods for a variety of across-the-stack measurements. By testing it under various conditions with different instrument parameters, valuable information can be obtained for the design of simpler, single-purpose gas-cell correlation instruments and to determine the factors that limit their performance.

By combining gas-cell correlation techniques along with dispersion techniques to carefully control the spectral bandpass, it has been possible to greatly improve the discrimination and the stability over that attainable with either technique used separately. A small, permanently aligned assembly employing a grating as the dispersing element is included for each of the 5 gases with the spectral bandpass selected to give optimum discrimination, stability, and signal-to-noise ratio. Each assembly uses a multiple-slit grid in the focal plane of the dispersed radiant energy to pass narrow spectral intervals that contain strong absorption by the gas. Discrimination and stability are improved by rejecting much of the energy at wavelengths where the gas does not absorb strongly. The improved discrimination against H_2O is particularly important when measuring NO. The instrument can be used with a grating assembly or without it, as in the more conventional manner.

Stack diameters between approximately 1.5 m and 10 m can be accounted for with only minor adjustments of a few optical components. In normal operation, the stack is "double-passed" by using a retroreflector on the side opposite the radiant energy source to reflect the energy back through the stack to the remainder of the instrument. However, by moving the source and some associated optics to the opposite side, it is possible to "single-pass" the stack.

The instrument has been tested in the laboratory with synthetic samples of effluent to provide calibration data at various temperatures and to measure the interference by other gases typically in stack effluent. Field tests have also been performed on the stack of a coal-burning power plant while the gas concentrations of interest were simultaneously being measured by other instruments. The data obtained on the stack and in the laboratory indicate that gas-cell correlation instruments can be built with adequate sensitivity and discrimination to monitor any of the 5 gases listed above. The ultimate performance of any instrument of this type for across-the-stack measurements will probably be limited by the uncertainty in determining and maintaining the "zero-balance" that corresponds to no absorbing gas in the stack. This is a much more serious problem for across-the-stack instruments than for instruments in which the sample area can be evacuated or flushed with a non-absorbing gas.

DEFINITIONS, SYMBOLS AND UNITS

T — transmittance at a particular wavenumber (or wavelength) that would be measured with a spectrometer having infinite resolving power. Subscripts indicate the transmittance of different components or gas samples. $\bar{T}$ indicates the average transmittance over a specified interval.

T_{sam} — transmittance of the sample gas being analyzed.

T_x — transmittance of the gas species x to be measured in the sample gas. This is equivalent to T_{sam} if only species x is present in the sample cell.

T_y — transmittance of an interfering gas of species y in the sample gas that may produce a false indication of species x.

T_f — transmittance of the spectral bandpass filter.

T_L — transmittance of the gas of species x at low pressure in a correlation cell.

T_{att} — transmittance of an attenuator, assumed to be constant over the spectral bandpass of interest.

T_H — transmittance of the gas of species x at high pressure in a correlation cell.

ν wavenumber of radiant energy (cm^{-1}).

ν_o wavenumber of the center of an absorption line. Other subscripts or superscripts indicate particular values. (cm^{-1}).

λ wavelength of radiant energy expressed in micrometers (μm).

f_c carrier frequency (high) (Hz).

f_a alternator frequency (low) (Hz).

p partial pressure of a particular gas species, usually species x (atm).

P total pressure of a gas mixture (atm).

ℓ geometrical path length of the radiant energy beam through a gas sample (cm).

C p/P, concentration of a gas species, usually expressed in parts per million (ppm) or percent.

u, w $p\ell$ (atm cm), absorber thickness of a particular gas species, u refers to gas in the sample cell and w to gas species x in a correlation cell. One atm cm is equivalent to 10^4 ppm meters.

k absorption coefficient at wavenumber ν of an absorption line $(atm\ cm)^{-1}$.

S $\int k d\nu$, intensity of an absorption line ($atm^{-1}\ cm^{-1}\ cm^{-1}$).

V_c voltage component of amplified detector signal at carrier frequency f_c.

V_a voltage component of amplified detector signal at alternating frequency f_a.

V' V_a/V_c, normalized voltage. Normalization is made so that V' = 1 when there is 100% modulation of the beam at frequency f_a. See Equation (5) and related text.

D.R. discrimination ratio, ratio of the concentration of an interfering gas species to the concentration of the species being measured that produces the same reading. This ratio may be positive or negative.

F $\lim_{u \to 0} \frac{V'}{u}$ Pembrook Factor $(atm\ cm)^{-1}$.

E chopped radiant energy. Equations (1) and (2) and related text define E_L and E_{att} and explain the subscripts.

M constant relating radiant energy to transmittances. See Equations (1) and (2).

Δ and Σ are defined and explained by Equations (3) and (4) and related text.

SECTION 2

SPECTROSCOPIC PRINCIPLES

CORRELATION IN SIMPLE SPECTRAL MODELS

Gas-cell correlation spectrometers of the type described here depend for their sensitivity on the correlation between the structure in the spectrum of the gas species x to be measured in the sample cell and that of the gas in a correlation cell. The desired correlation is achieved by filling the correlation cell with the same gas species x. Generally, the spectral bandpass of the instrument includes several absorption lines so that the gas in the correlation cell has large fluctuations in the transmittance at different wavenumbers. Figures 1-4 are based on a simple instrument and a greatly simplified model spectrum to illustrate the spectroscopic principles of detection and discrimination in such a way that the reader can easily follow the mathematics involved.

An optical diagram of a simple gas-cell correlation spectrometer is illustrated in Figure 1. Radiant energy from a source passes through either a correlation cell or an attenuator, then through the sample cell and a bandpass filter to the detector. The sample cell may be a stack or a closed cell with windows, or it may simply be an open space such as an atmospheric path. The correlation cell is filled with gas species x to be measured. The attenuator and the correlation cell are alternately moved into the beam at the alternator frequency f_a. An ac amplifier measures the component of the detector signal at frequency f_a that results from a difference between the amounts of radiant energy on the detector during the two halves of the alternator cycle.

For simplicity, we assume that the transmittance of the bandpass filter is unity from wavenumber ν_a to $\nu_a + 1\ cm^{-1}$, and is zero elsewhere. A transmission spectrum of the gas in the correlation cell is illustrated in the upper-left corner of Figure 2. The upper-right portion shows the transmittance spectrum of the attenuator over the same spectral region. Note that $\bar{T}_L$, the average transmittance of the correlation cell, is made equal to $\bar{T}_{att}$, the average transmittance of the attenuator. When there is no absorbing gas in the sample cell, the amplifier output is zero because the amount of radiant energy incident on the detector is the same during both halves of alternator

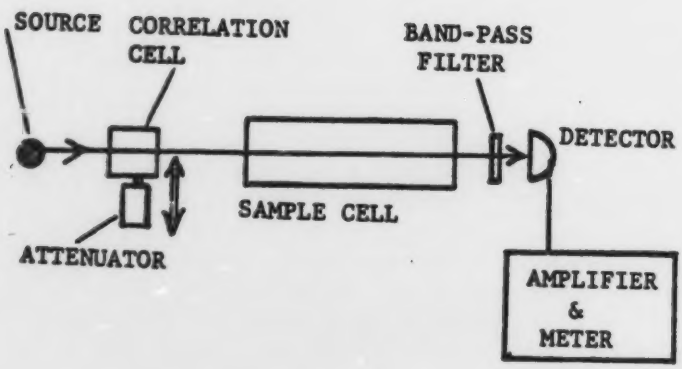

FIG. 1. Simplified optical diagram of a basic gas-cell correlation spectrometer.

cycle. A sample of gas of species x in the sample cell is represented by the middle panel of Figure 2. Because the same gas species exists in both the correlation cell and the sample cell, the absorption occurs over the same spectral interval in both cells. The difference in the transmittance results from different amounts of gas in the two cells.

The transmittance of the correlation cell and the sample in series is given by $T_L \cdot T_{sam}$. In this case, the sample does not affect the transmittance because the correlation cell absorbs all of the energy at wavenumbers where the sample absorbs. During the correlation-cell half of the alternator cycle, the energy on the detector is proportional to $\int T_L \cdot T_{sam}\, d\nu$, which is numerically equivalent to $\overline{T_L \cdot T_{sam}}$ in the 1 cm^{-1} interval. The lower right-hand portion of Figure 2 illustrates the spectrum of the energy during the attenuator-half of the cycle. Note that the two halves are no longer balanced with the sample cell. $\overline{T_L \cdot T_{sam}} = 0.50 > \overline{T_{att} \cdot T_{sam}} = 0.375$. The difference is measured by the a.c. amplifier and meter and is related to the concentration of the gas in the sample. Because T_{att} is a constant equal to $\overline{T_L}$, $\overline{T_L \cdot T_{sam}} = \overline{T_{att} \cdot T_{sam}} = \overline{T_{att} \cdot T_{sam}}$. When there is a positive correlation between the spectral structures of the gases in correlation cell L and the sample cell, $\overline{T_L \cdot T_{sam}} > \overline{T_L} \cdot \overline{T_{sam}}$, as in the example above. If $\overline{T_L \cdot T_{sam}} < \overline{T_L} \cdot \overline{T_{sam}}$, the correlation is negative. The two terms are equal when there is no correlation.

Figures 3 and 4 are based on the same correlation cell and attenuator as the previous example and illustrate the interference by two different absorbing gas species other than species x in the sample. The gas species illustrated in the upper panel of Figure 3 absorbs, but at different wavelength numbers than does species x. The correlation between the spectra of the sample and species x is obviously negative with the resulting misbalance opposite to that when only species x is in the sample. $\overline{T_L \cdot T_{sam}} = 0.40 < \overline{T_{att} \cdot T_{sam}} = 0.45$. If the interfering gas is alone in the sample cell, as indicated by Figure 3, the instrument will indicate a negative amount of species x. When both species x and the interfering gas are present, the indicated concentration of species x is too low.

The interfering gas of species y illustrated in Figure 4 has two absorption lines, one inside the absorption line of species x and one outside. No correlation exists between the spectra of this gas and species x, and $\overline{T_L \cdot T_y} = 0.4 = \overline{T_{att} \cdot T_y}$. The interfering gas decreases, by the same fraction, the energy incident on it during both halves of the cycle, and the system remains balanced. The lower panels of Figure 4 correspond to a sample consisting of species y, whose transmittance is plotted in the upper panel, and species x, represented by the middle panel of Figure 2. We note that $\overline{T_L \cdot T_{sam}} - \overline{T_{att} \cdot T_{sam}} = 0.4 - 0.3 = 0.1$. This difference is less than the 0.125 produced by the same amount of species x, but with no species y present (Figure 2). Although the interfering gas y by itself does not produce a misbalance, it reduces the misbalance produced by species x to 0.8 its original value. This factor is, of course, equal to $\overline{T_y}$.

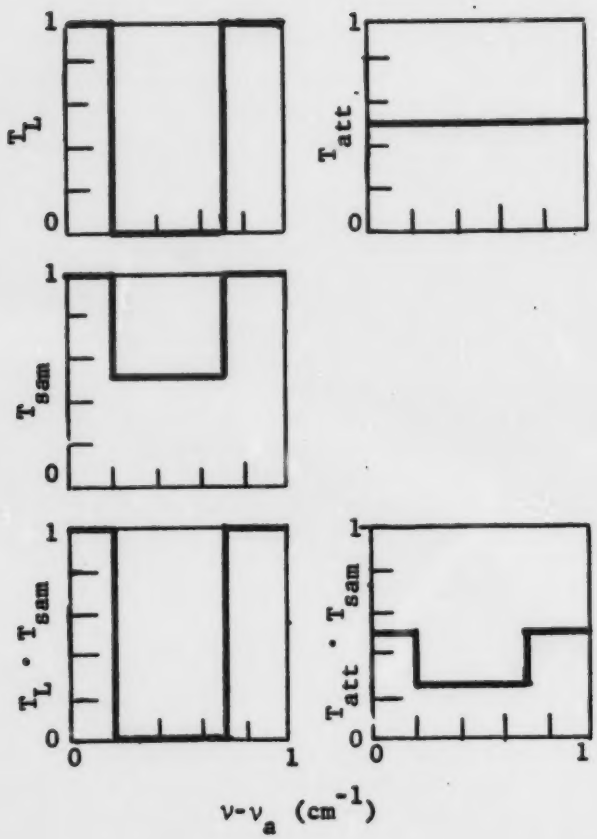

FIG. 2. Plots of transmittance for a model gas illustrating the spectroscopic principles of detection. The average transmittances are as follows:

Upper panels, $\overline{T}_L = 0.50$ and $\overline{T}_{att} = 0.50$. Middle panel, $\overline{T}_{sam} = 0.75$.

Lower panels, $\overline{T_L \cdot T_{sam}} = 0.50$ and $\overline{T_{att} \cdot T_{sam}} = 0.375$.

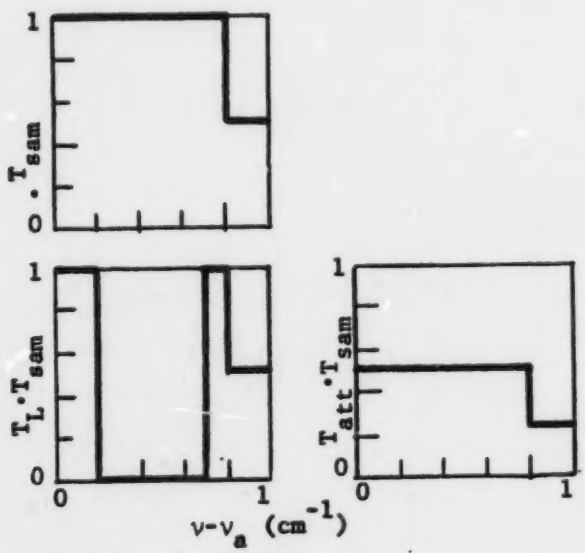

FIG. 3. Plots of transmittance illustrating interference by a gas species other than the one being measured.

Upper panels, $\overline{T}_{sam} = 0.9$. Lower panels, $\overline{T_L \cdot T_{sam}} = 0.40$ and $\overline{T_{att} \cdot T_{sam}} = 0.45$.

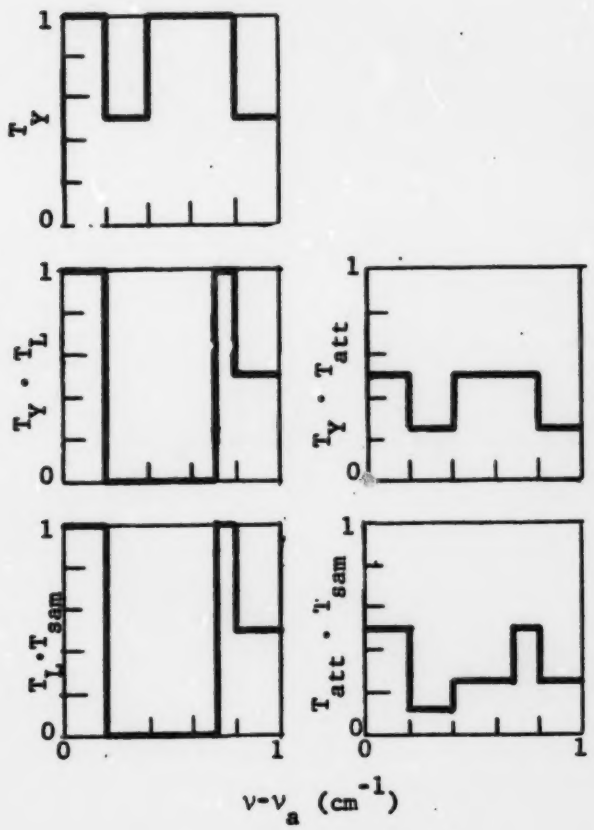

FIG. 4. Plots of transmittance illustrating the effect of an absorbing gas of species y whose spectrum is not correlated with that of species x. The upper panel represents gas species y alone in the sample cell. The combined transmittances of species y with the correlation cell and with the attenuator are shown in the two middle panels. The corresponding two plots in the two lower panels are for a sample consisting of both species x and species y.

Upper panels, $\overline{T}_y = 0.80$. Middle panels, $\overline{T_L \cdot T_y} = 0.40$ and $\overline{T_{att} \cdot T_y} = 0.40$. Lower panels, $\overline{T_L \cdot T_{sam}} = 0.40$ and $\overline{T_{att} \cdot T_y} = 0.30$.

A similar reduction in the misbalance due to a sample of species x would be produced by continuum absorption or by dirt on the windows of the sample cell. The reduction in the misbalance and in the resulting detector signal can be accounted for by processing the detector signal in such a way that the output is proportional to $(\overline{T_L \cdot T_{sam}} - \overline{T_{att} \cdot T_{sam}})/(\overline{T_L \cdot T_{sam}} + \overline{T_{att} \cdot T_{sam}})$. For example, from Figure 2, we see that this ratio for species x, $(0.50 - 0.375)/(0.50 + 0.375) = 1/7$, is equal to the corresponding ratio for the same quantity of species x plus the uncorrelated species y represented by Figure 4: $(0.40 - 0.30)/(0.40 + 0.30) = 1/7$. The instrument described in the following section measures a quantity proportional to this ratio. In most real situations, the spectral band includes several absorption lines of the gas being measured and may include several lines of one or more interfering gases. If the positions and intensities of the lines of the interfering gas are completely uncorrelated with those of species x, the interfering gas will behave as the one illustrated in Figure 4 and not produce a false indication. In practice, the spectrum of a gas absorbing within the spectral bandpass will usually have some correlation either positive or negative, with that of species x and consequently will interfere with the measurement.

ENERGY AND VOLTAGE RELATIONSHIPS

Figure 5 illustrates a gas-cell correlation spectrometer that is more complex than the basic one shown in Figure 1. It is similar in operating principle to the one built by us for across-the-stack measurements and can be used with two correlation cells or with one correlation cell and an attenuator. The alternator consists of correlation cell L and either an attenuator or correlation cell H along with the optical and mechanical components that alternately direct the beam through them. The one-cell attenuator system employs correlation cell L and an attenuator. In the two-cell system, the attenuator is replaced by correlation cell H, which contains the gas species to be measured at high pressure. In the alternator, the beam may remain fixed while the correlation cells (or attenuator) move as indicated, or the correlation cells may remain fixed while the beam is alternately directed through them by moving mirrors. In either case, the beam passes through the sample cell during both halves of the attenuator cycle.

Before passing through the alternator, the energy beam is chopped at a relatively high frequency f_c, called the carrier frequency. The difference in the energy during the two halves of the alternator cycle modulates the amplitude of the carrier signal. Employing the high frequency chopping in addition to the low frequency modulation makes it possible to measure a quantity proportional to V_a/V_c, where these voltages are proportional to the components of the detector signal at frequencies f_a and f_c, respectively. The ratio V_a/V_c can be related experimentally to the gas concentration and is relatively independent of the source brightness, detector sensitivity, dirt on windows or mirrors, etc.

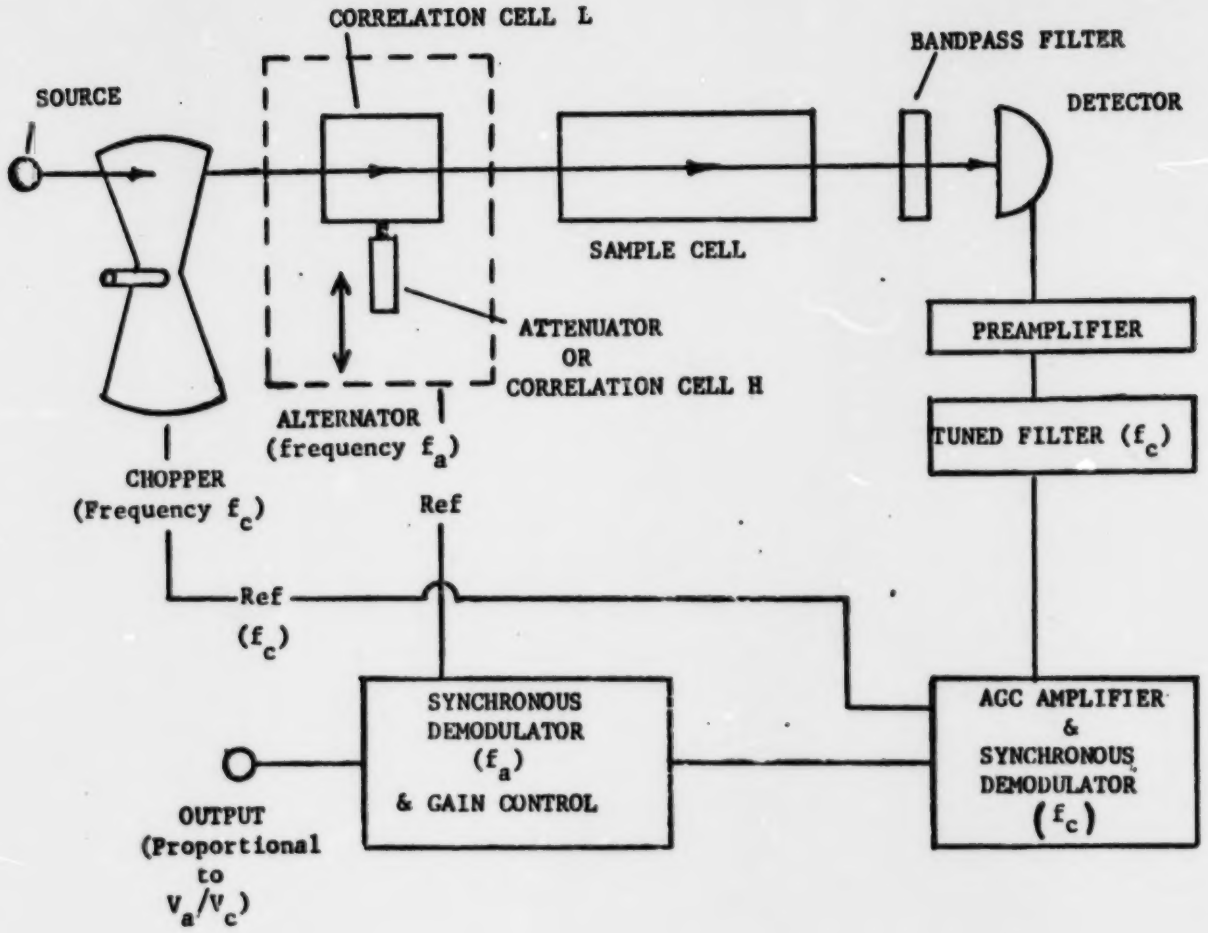

FIG. 5. Simplified diagram of a gas-cell correlation spectrometer that employs high-frequency chopping and low-frequency modulation.

Figure 6 contains several plots of calculated transmittance for a model spectrum used to illustrate the spectroscopic principles of the one cell-attenuator system illustrated in Figure 5. The curves correspond closely to those of Figure 2, except that the rectangular-shaped spectral lines of Figure 2 are replaced by two absorption lines with spacings, intensities, and half-widths typical of a portion of the fundamental CO band. The curves of Figure 6 are quite realistic, but the effects of correlation are less obvious than in Figure 2. For simplicity, we assume that the bandpass filter passes only the spectral region between the centers of the absorption lines ($T_f = 1$ for $0 \leq \nu - \nu_a \leq 4$ cm^{-1}, and $T_f = 0$ for all other ν).

The radiant energy chopped at frequency f_c incident on the detector during the half-cycle that the correlation cell L is in the beam is given by

$$E_L = M \int T_f \, T_L \, T_{sam} \, d\nu. \tag{1}$$

The corresponding energy during the attenuator-half of the cycle is

$$E_{att} = M \int T_f \, T_{att} \, T_{sam} \, d\nu. \tag{2}$$

Although T_f is constant in the present example, it is left under the integral sign so that the equations will be valid for all situations. The constant M depends on source intensity and size, aperture sizes, window transmittance, mirror reflectivities, etc. For simplicity, we assume that the spectral emissivity of the source and sensitivity of the detector are both constant over the spectral interval of interest. The remainder of the discussions on spectroscopic principles is based on the condition that $E_L = E_{att}$ with no sample in the sample cell. ($T_{sam} = 1$.)

The curve in the upper panel of Figure 6 labeled ($T_{att} - T_L$) represents the spectral response of the system at frequency f_a. Sample absorption where ($T_{att} - T_L$) >0 produces a positive V_a. On the other hand, a gas in the sample cell with a strong absorption line where ($T_{att} - T_L$) < 0 and no absorption where this quantity is > 0 would have a negative correlation with the gas in the correlation cell and would produce a negative V_a. If the spectrum of the sample gas is completely uncorrelated with the spectrum of the gas in the correlation cell, the absorption producing negative V_a balances that producing positive V_a.

The spectrum shown in the center panel of Figure 6 corresponds to 0.01 atm cm of CO at 1 atm pressure in the sample cell. During the half of the cycle when correlation cell L is in the beam, the transmittance of the beam that has passed through the sample is given by $T_L \cdot T_{sam}$. This quantity is indicated in the lower panel along with the corresponding curve that applies during the attenuator-half of the alternator cycle. The sample absorbs only a very small portion of the radiant energy that has passed through correlation cell L because little energy remains at the wavenumbers where the sample absorbs. During the attenuator half of the cycle, the sample absorbs a larger portion of the energy with the result that $E_L > E_{att}$. A detector voltage component V_a proportional to ($E_L - E_{att}$) appears as a modulation of the carrier voltage V_c.

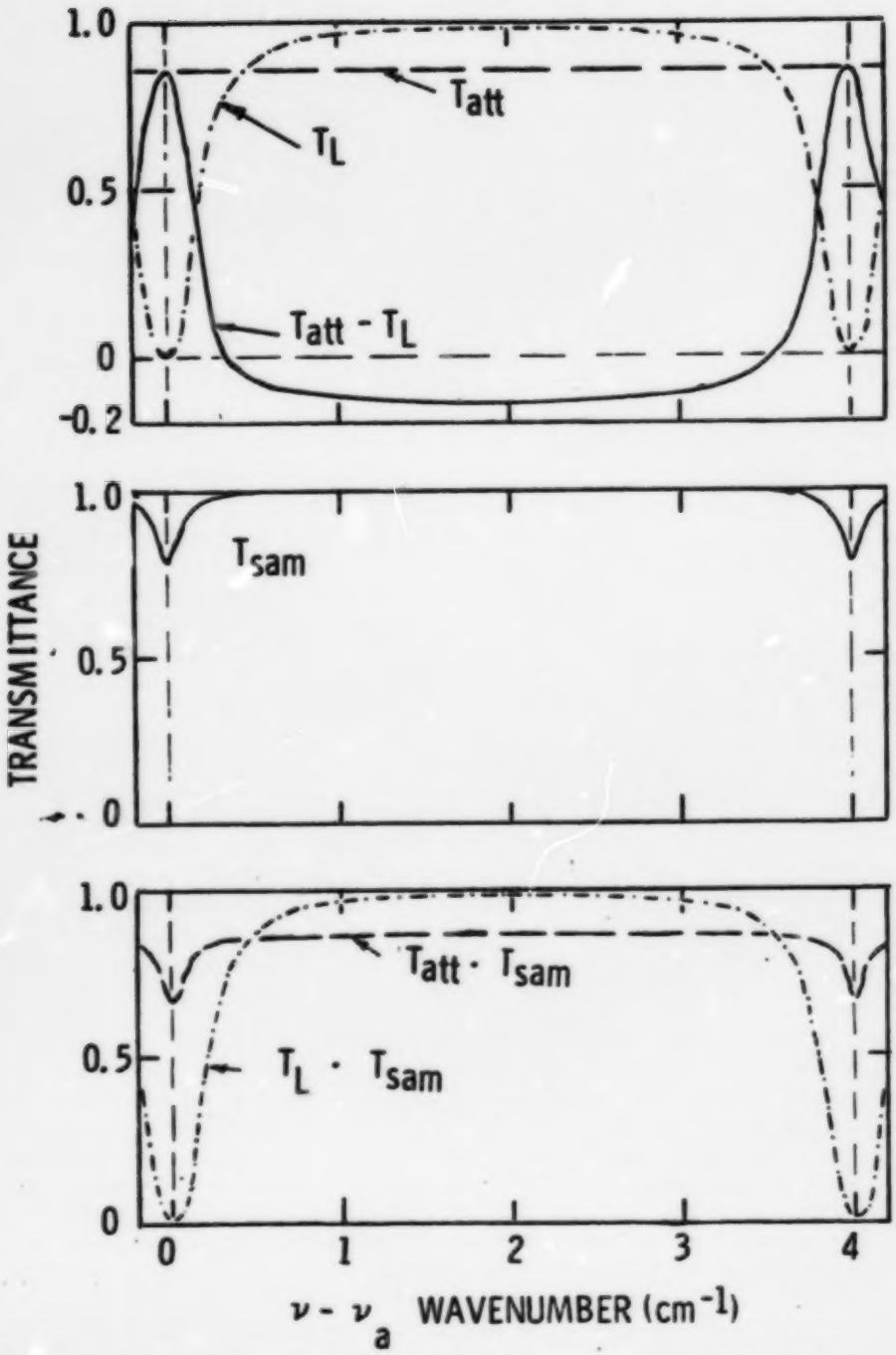

FIG. 6. Calculated spectral plots of transmittance for a model spectrum similar to a portion of a CO band. The curves illustrate the principle of detection of the one cell-attenuator system. The plot of T_L is based on a correlation cell containing 0.2 atm cm of CO at 1 atm pressure.

The curves in Figure 7 illustrate the dependence of E_{att} and E_L on sample absorber thickness for the spectral model illustrated in Figure 6. Each pair of curves correspond to a different absorber thickness w of species x in the correlation cell; the pressure is maintained at 1 atm. Because $T_f = 1$ over the region of interest, $0 \leq \nu - \nu_a \leq 4\ cm^{-1}$, $\overline{T_L \cdot T_{sam}} = E_L/4M$, and $\overline{T_{att} \cdot T_{sam}} = E_{att}/4M$. As the sample absorber thickness u approaches zero, T_{sam} approaches unity, and $\overline{T_L \cdot T_{sam}}$ and $\overline{T_{att} \cdot T_{sam}}$ approach $\overline{T_L} = \overline{T_{att}}$.

We define two useful quantities.

$$\Delta = \int T_f(T_L - T_{att})\, T_{sam}\, d\nu = (E_L - E_{att})/M. \tag{3}$$

$$\Sigma = \int T_f(T_L + T_{att})\, T_{sam}\, d\nu = (E_L + E_{att})/M. \tag{4}$$

For the spectral model of Figure 6, Δ is proportional to V_a and to the difference between values plotted in Figure 7 for given values of u and w. Similarly, Σ is proportional to the sum of the same values and to the average value of V_c. Neither Δ nor Σ is easy to measure directly; however, the ratio can be measured with an instrument of the kind illustrated in Figure 5. In order to calibrate the instrument, the radiant energy beam through the attenuator is temporarily blocked so that T_{att} and, in turn, E_{att}, equal zero. Under this condition $\Delta/\Sigma = 1$, and the amplifier gain settings are adjusted so that the output voltages V_a and V_c are equal. We define

$$V' = V_a/V_c \tag{5}$$

with the gain settings adjusted as just described. If the gain settings remain fixed, it follows that $V' = V_a/V_c = \Delta/\Sigma$ when the attenuator beam is unblocked and the voltages are measured.

An automatic gain control circuit that maintains V_c constant can further simplify the measurement. When this is used, V' is proportional to V_a, which is measured directly. Thus, only one voltage, V_a, need be read in order to determine Δ/Σ.

Curves based on calculated values of $V' = \Delta/\Sigma$ are shown in Figure 8 for 5 values of w, including the 2 represented in Figure 7. Recall that the calculated curves are based on a portion of a model spectrum similar to a CO spectrum and that the spectral interval corresponds to the spacing between two adjacent lines. Because the curves of Figure 8 are based on ratios of integrated transmittance, it follows that the same curves would be obtained if the spectral interval of the model spectrum were widened to include several identical lines with the same spacings. Such a model is similar to the 8 or 10 strongest lines in either the P branch or the R branch of the fundamental CO band. We have employed a gas-cell correlation spectrometer with a spectral bandpass that included approximately 10 of the strongest lines in the R branch of the CO band. Each experimental curve we obtained was very similar to the one for the corresponding value of w in Figure 8. The differences between the experimental and the calculated curves could be explained

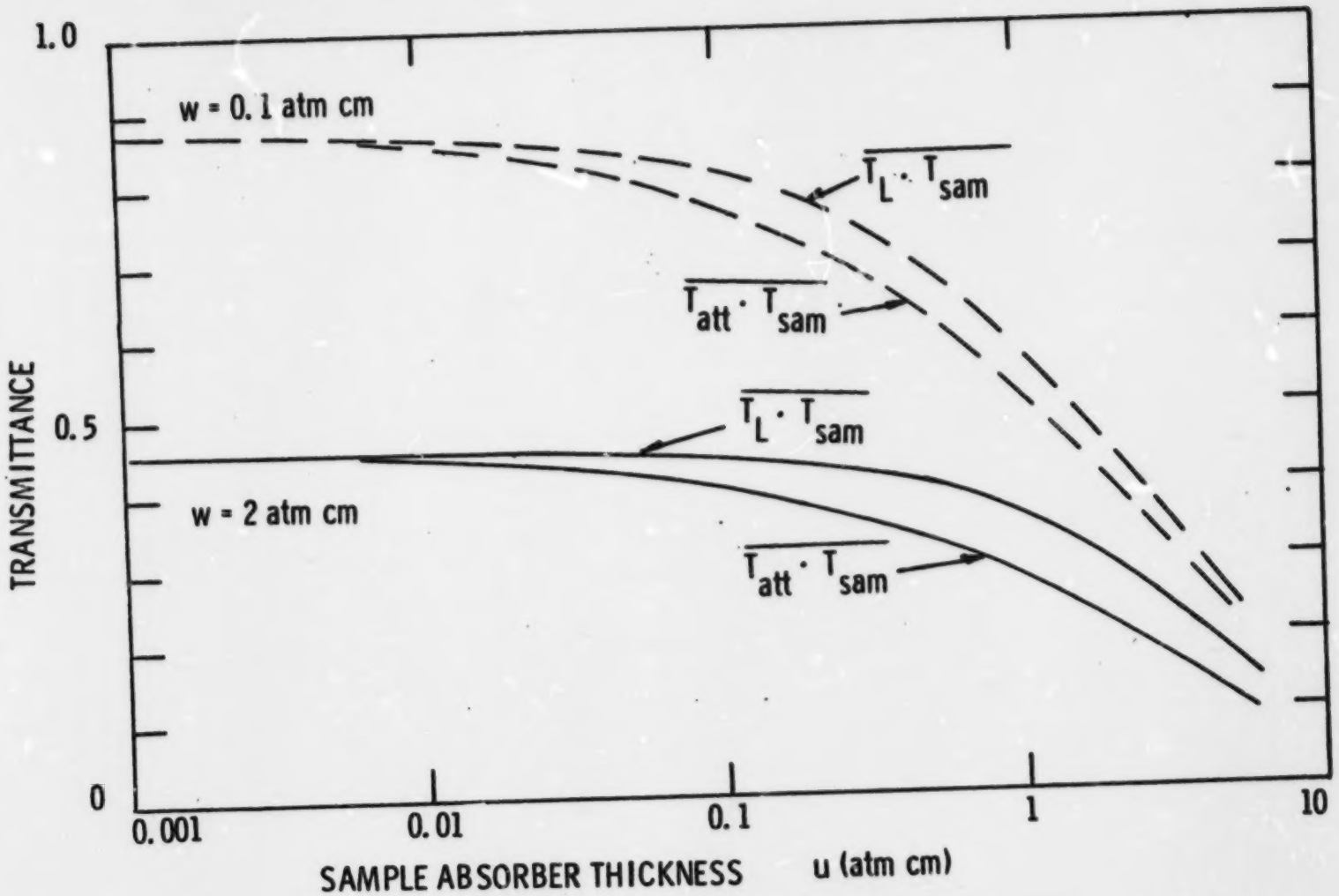

FIG. 7. Plots of calculated $\overline{T_L \cdot T_{sam}}$ and $\overline{T_{att} \cdot T_{sam}}$ versus sample absorber thickness. The curves are based on the spectral model similar to CO that is illustrated in Fig. 6.

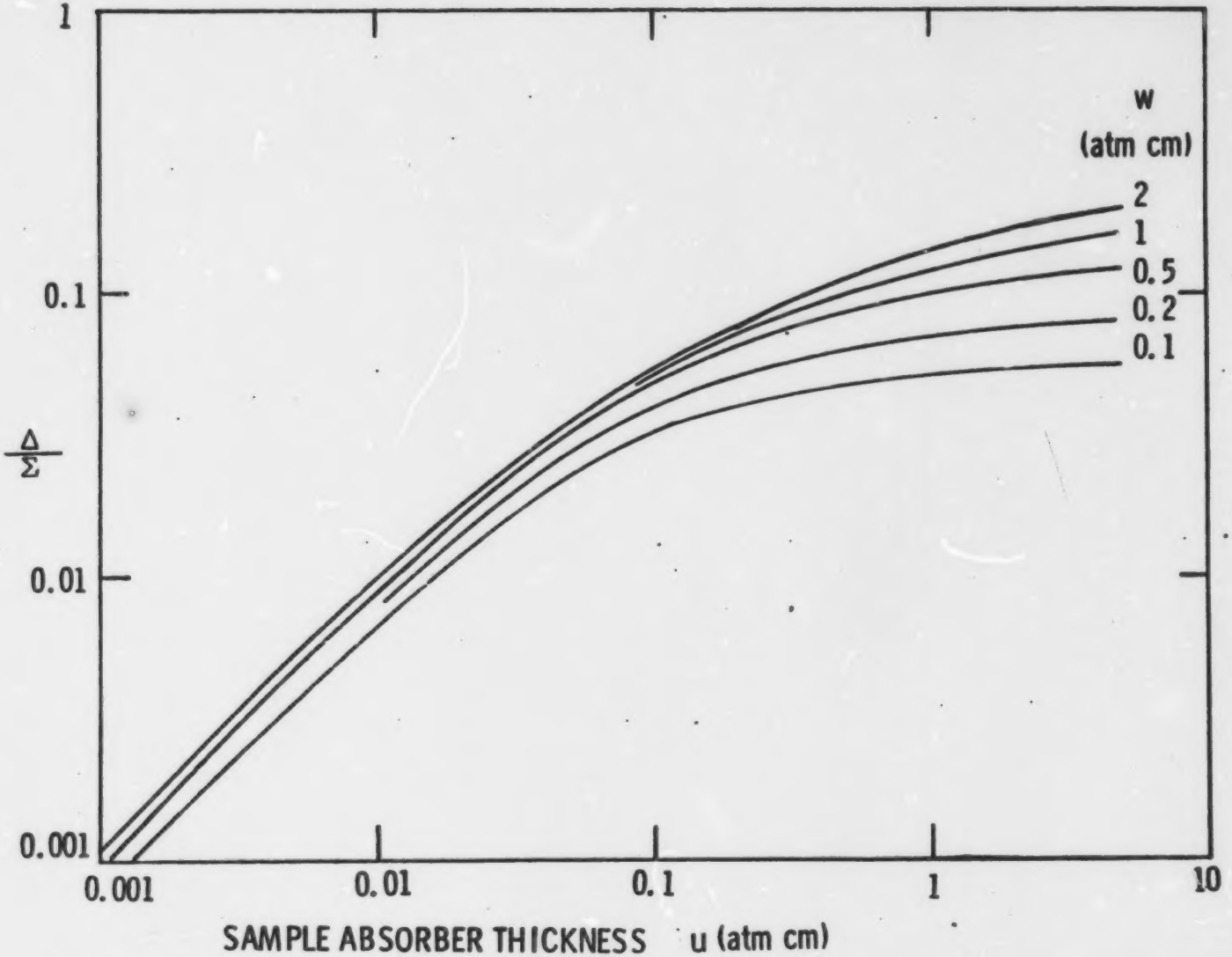

FIG. 8. Plot of calculated Δ/Σ versus sample absorber thickness. Each curve is identified by w, the absorber thickness of gas species x in correlation cell L. $\overline{T}_L$ for each value of w is: 2 atm cm, 0.461; 1 atm cm, 0.600; 0.5 atm cm, 0.711; 0.2 atm cm, 0.817; and 0.1 atm cm, 0.875.

by the difference between the model spectrum and the real CO spectrum and by the shape of the transmission curve of the bandpass filter used in the instrument. A "rectangular" bandpass in which $T_f = 0$ or 1 has been assumed for the calculations.

An experimental curve of V_a vs u can be obtained without adjusting the amplifier gains by the procedure described above. The shape of the curve on a logarithmic scale is the same regardless of changes in the gain setting, which shift the curve vertically. However, adjusting the gains as outlined makes it possible to relate V_a directly to Δ/Σ. For small values of u, the curves of Figure 8 have unity slope, indicating that Δ/Σ is proportional to u. Furthermore, for a given value of u, Δ/Σ varies by a factor of only about 1.5 for variations of a factor of 20 for w.

If w were further reduced to values much less than those indicated, T_L would no longer approximate zero near the line centers, and Δ/Σ would reduce more rapidly. In many situations, the major factor limiting the accuracy of a gas-cell correlation instrument is "zero-drift", the slow variation in the signal output when u = 0. An important instrumental parameter is given by

$$F = \lim_{u \to 0} \frac{V'}{u} = \lim_{u \to 0} \frac{\Delta}{u\Sigma} \quad (\text{atm cm})^{-1}. \tag{6}$$

For lack of an unambiguous and descriptive name, we have named F the Pembrook Factor after one of our colleagues, John Pembrook, who has done considerable work in developing methods to evaluate instrument performance. For example, from Figure 8 we see that $\Delta/\Sigma \cong 0.001$ when u = 0.001 atm cm and w = 1 atm cm. Thus, $F = 1.00\ (\text{atm cm})^{-1}$, and a zero-drift corresponding to a misbalance of $\Delta/\Sigma = 0.001$ produces an error equivalent to 0.001 atm cm of the gas being measured. From Equations (3) and (4), we see that this corresponds to a zero-drift such that 0.998 as much chopped radiant energy is transmitted through the alternator during one-half of its cycle as during the other half. $[(1 - 0.998)/(1 + 0.998) \cong 0.001]$. It follows that the spectral bandpass and correlation cell parameters should be chosen to produce a large value of F if the sample cannot be removed so that zero drift can be checked and accounted for regularly.

The slopes of the curves of Figure 8 decrease with increasing u. For values of u more than 1 or 2 times w, the dependence of V' on u is so slight that it establishes a practical upper limit of u for an instrument.

DESIGN FACTORS

From Figures 6, 7, and 8, we can establish some general "rules of thumb" and factors to be considered in determining the optimum spectral bandpass, sample cell length, and correlation cell parameters for a particular application. The spectral bandpass should be chosen to include strong absorption lines of gas species x to be measured and a minimum of absorption by other gas species that may be present in the sample gas. Interference by other gas species can generally be decreased by employing a selected narrow bandpass. However, a lower practical limit on the width of the spectral bandpass may be determined by filters that are available or by detector noise. If the bandpass is very narrow, the signal output, which is proportional to Δ, (Equation (3)) for small u may be less than the detector noise.

The absorber thickness w in the correlation cell should be great enough that the gas is essentially opaque at the wavenumber of strong absorption near the line centers. The curves of Figure 8 show that by employing a relatively large w, a larger Pembrook Factor F can be achieved along with an extension of the dynamic range to larger values of u. Two factors establish a practical upper limit on w. If the correlation cell is opaque over too wide of a spectral interval near each line center, the "sharp" structure is lost and discrimination against other gases may suffer. Furthermore, as w increases to the point that T_L is small, the signal output resulting from a small u decreases, and detector noise may become a problem. The decrease in signal output with increasing w can be observed in Figure 7 in which Δ is proportional to the separation between a pair of curves. For a given u less than approximately 0.1 atm cm, Δ is larger for w = 0.1 atm cm than for w = 2 atm cm. If w were increased further, Δ would continue to decrease, but the ratio Δ/Σ would continue to increase slightly as indicated in Figure 8 because Σ would also decrease.

The optimum combination of sensitivity and discrimination are generally achieved when the pressure of the gas in the low pressure correlation cell is equal to or somewhat less than the pressure in the sample cell. This ensures that the widths of the pressure-broadened lines are approximately the same in both cells. We have shown experimentally and analytically that the performance is seldom affected significantly when the correlation cell pressure varies from the sample pressure down to less than half of its value. If the spectral bandpass contains only spectral lines of approximately equal intensity, the dependence on pressure is less than if the lines cover a wide range of intensities. It is understood that as the pressure is varied, the absorber thickness is adjusted to maintain near opacity near the centers of the strong lines. The desired combination of total pressure and absorber thickness is achieved by varying the length of the correlation cell or by adding a non-absorbing gas such as N_2 to collision broaden the lines.

For a fixed sample cell length, the range of concentrations that can be measured is limited on the low end by noise or by uncertainty in the correct zero reading and on the upper end by the "saturation" indicated by the curves of Figure 8. If it is practical, the sample cell length is selected to be consistent with the range of concentrations to be measured. Two or more sample cell lengths may be required to cover the entire range of concentrations. In some applications, such as across-the-stack measurements of stationary source pollutants, the optical length through the sample gas may be difficult to change. Double-passing the energy beam through a stack to increase the length may be practical but limits on window sizes and on the mechanical stability of the optical platforms make it difficult to pass the beam across the stack more than twice. If one pass of the stack produces too much absorption, it may be necessary to select a different spectral bandpass in which the absorption is weaker. Another solution is to use an optical arrangement that passes the radiant energy beam across only part of the stack. This method does not provide the averaging of a path that extends across the entire stack.

Narrowing the absorption lines by decreasing the sample pressure to less than 1 atmosphere can greatly improve the discrimination and sensitivity for some gases. This is particularly true for SO_2, whose absorption lines are so closely spaced that they overlap and smooth out much of the spectral structure when the sample is near 1 atm. At pressures less than about 0.1 atm, the spectral structure of SO_2 is greatly increased so that the performance of a gas-cell correlation spectrometer is improved. The optimum sample cell length and correlation cell parameters for any application obviously depend on the sample pressure. The half-width of a collision-broadened absorption line is proportional to the total gas pressure and inversely proportional to the square root of the temperature. Therefore, the spectral lines of a hot gas in a smokestack are narrowed by the higher temperature although the pressure is approximately atmospheric.

TWO-CELL SYSTEM

The two-cell system is illustrated schematically by Figure 5 when a high-pressure correlation cell H is used in place of the neutral density attenuator. Figure 9 illustrates the spectroscopic principles of this system with the same low-pressure sample in correlation cell L as in the case illustrated in Figure 6. The model is based on correlation cell H filled to 5 atm with CO, the gas to be detected. The absorber thickness of the CO in this cell, 0.108 atm cm, was adjusted so that $\int T_f T_H d\nu = \int T_f T_L d\nu$. Because of the pressure broadening of the absorption lines, the gas in cell H absorbs less near the centers of the lines, but more in the wings of the lines, than does the low-pressure gas in cell L. The curve labeled $(T_H - T_L)$ represents the spectral response of the system at frequency f_a. By comparing Figure 9 with Figure 6, we see that the response $|T_H - T_L|$, of the two-cell system is less than $|T_{att} - T_L|$, of the one-cell attenuator system in the region midway between the lines. Thus, the two-cell system would discriminate better against an absorption line of an interfering gas in this region. The two-cell system is only about 3/5 as sensitive as the one cell-attenuator system because of the smaller value of $(T_H - T_L)$ near the centers of the lines.

In matching $\int T_f T_L d\nu$ with $\int T_f T_H d\nu$, the pressure of the gas in cell H could have been made higher with a corresponding shorter path to maintain the balance between the two beams. This change would further broaden the lines, increasing T_H near the line centers and decreasing it in the wings. As a result, the spectral response would be greater near the centers of the lines. However, this would be accompanied by an increased negative response in the wings of the lines, causing the system to respond more to absorption by other gases with absorption lines between the CO lines. The optimum pressure in the cells depends on the spectra of the gas species to be measured and any interfering gases in the sample. In many cases, the decrease in response of the two-cell system is more than compensated for by an increased discrimination over the one cell-attenuator system.

Figure 10 illustrates model spectra for which the discrimination by the two-cell system is far superior to that by the one cell-attenuator system. The curves labeled T_L and T_H in the upper panel correspond to the transmittances of low and high pressure correlation cells, respectively. Both have

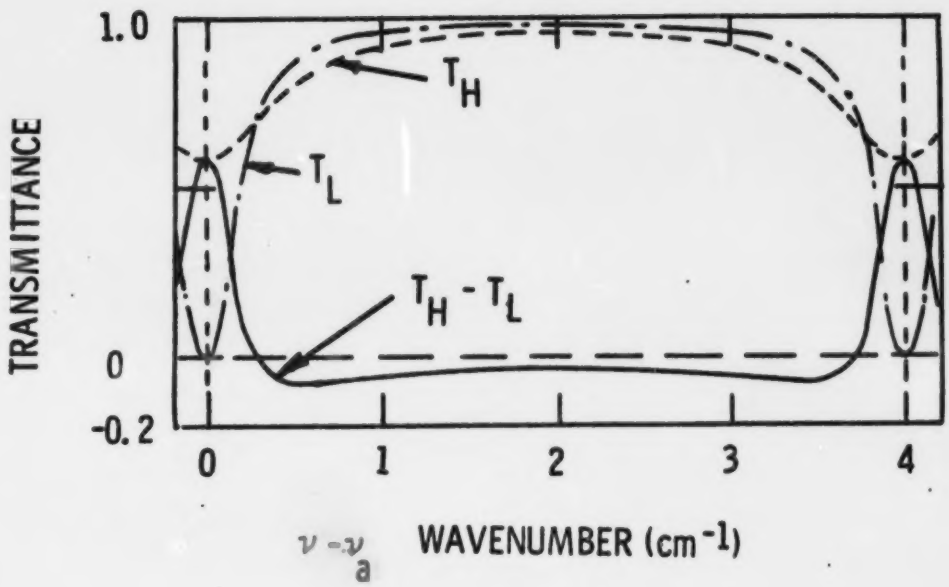

FIG. 9. Calculated spectral plots of transmittance for a model spectrum illustrating the principle of detection of the two-cell system.

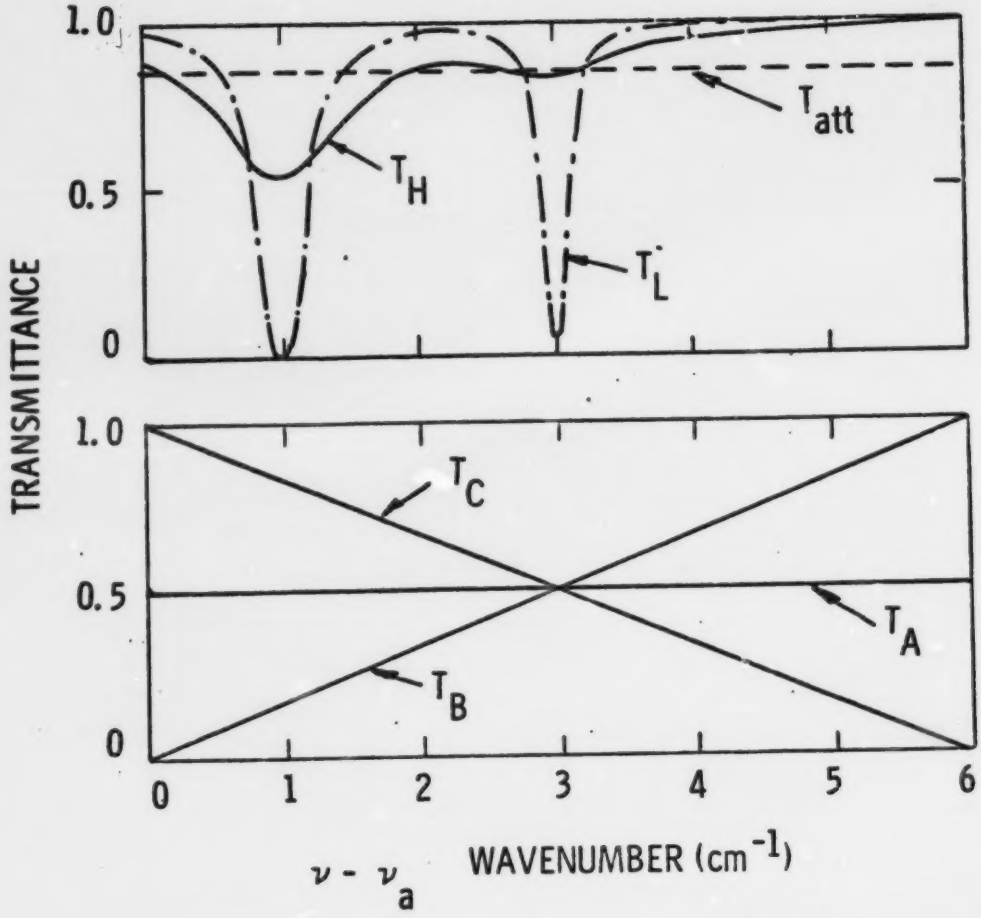

FIG. 10. Calculated spectral plots of transmittance demonstrating the principles of discrimination against continuum absorption by the two-cell and the one-cell attenuator systems.

same average transmittance, which is represented by the curve labeled T_{att}. Thus the two curves T_L and T_H correspond to the two-cell system, and the curves T_L and T_{att} correspond to the one-cell attenuator system. Both of the absorption lines have a half-width α of 0.05 cm^{-1} for the low pressure sample, and 0.5 cm^{-1} for the high pressure sample. The intensities of the lines at $(\nu-\nu_a)$ = 1, and 3 cm^{-1} are 4 $atm^{-1}cm^{-1}cm^{-1}$ and 1 $atm^{-1}cm^{-1}cm^{-1}$, respectively. The absorber thicknesses of gas x in the low and high pressure cells are 0.5 and 0.24074 atm cm, respectively. It is assumed that $T_f = 1$ for $0 \leq (\nu-\nu_a) \leq 6$ cm^{-1} and $T_f = 0$ for all other ν.

Curves A, B and C in the lower panel represent three simple types of continuum absorption by interfering gases in the sample. Table 1 summarizes the relative sensitivities of the two systems to the three types of continuum and to a small amount of gas species x at the same pressure as the gas in correlation cell L. The equivalent error corresponds to the amount of gas species x that produces the same Δ/Σ as that produced by the interfering continuum. Continuum A has constant transmittance and produces no error, whereas Continua B and C produce signals in the one-cell attenuator system that correspond to a sample containing approximately 0.108 atm cm of the gas x. The equivalent error for the two-cell system is only about 2% as much. Sample B produces an error that corresponds to a positive amount of gas x because the general slope of the transmittance curve is similar to that of gas x; i.e., the transmittance increases with increasing wavenumber for both gas x and continuum B. As expected, the opposite is true for continuum C, whose transmittance curve slopes in the opposite direction.

A small amount of gas species x produces a smaller signal in the two-cell system than in the one-cell attenuator system; however, the increase in discrimination may be more important than the loss in sensitivity. Similar results would be obtained if the continua were replaced by spectra with the same general slopes, but consisting of many lines. Thus, curves B or C may be representative of the spectra near the edge of an absorption band of an interfering gas. The model spectrum of gas x in the correlation cells is also typical of the edge of many absorption bands in which the lines get progressively weaker with increasing distance from the band center. As an example, interference by the wing of a CO_2 band when measuring CO is similar to the model illustrated in Figure 10. In such a case, the discrimination by the two-cell system can be much better than that by one-cell attenuator system.

TABLE 1

COMPARISON OF THE SENSITIVITY AND DISCRIMINATION
OF TWO-CELL AND ONE-CELL ATTENUATOR SYSTEM

Sample	Two-Cell		One-Cell Attenuator	
	$\frac{\Delta}{\Sigma}$	Equivalent Error (atm cm)	$\frac{\Delta}{\Sigma}$	Equivalent Error (atm cm)
0.001 atm cm of gas	0.0002066		0.0003203	
Continuum A	0	0	0	0
Continuum B	0.0004778	+0.00231	0.03474	+0.1084
Continuum C	-0.0004778	-0.00231	-0.03474	-0.1084

MULTIPLE CORRELATION CELL SYSTEMS

The discussion above has been restricted to relatively simple instruments for which the processing of the detector signal is not excessively complicated. By using more than two correlation cells with different amounts of gas either at different pressures or at the same pressure, it may be possible to obtain more information about the sample absorption and to better account for interfering gases, particulate matter, and variations in sample temperature or pressure. In general a measurement with a correlation cell containing a small amount of gas at low pressure provides information about the absorption near the centers of the lines. Similarly, a correlation cell with more gas absorbs over a wide interval near the line centers and provides information about absorption in the wings of the lines. An alternate method is to use a single correlation cell and vary the gas pressure in it. Processing the detector signal for an instrument with more than two correlation cells, or with one of varying pressure, is necessarily more complicated than for two cells or for one cell and an attenuator. The added complication is usually not required for absorption measurements, but it may be justified for passive measurements in which the hot gas being measured serves as the radiant energy source.

SECTION 3

INSTRUMENT DESIGN AND PERFORMANCE

OPTICAL LAYOUT OF BASIC INSTRUMENT

Figure 11 shows the optical diagram of the instrument that was built and tested for EPA. It employs the principles described above and can be used to compare different methods of gas-cell correlation spectroscopy under a variety of situations. Different gas species can be measured by interchanging the gas correlation cells, a bandpass filter, and possibly the source and detector. The instrument is equipped with correlation cells and filters to measure NO, CO, SO_2, HCl, or HF. All of the optical components shown in Figure 11 are mounted on a baseplate approximately 47 cm x 53 cm. Except for a preamplifier, all of the electronic components are mounted separate from the optics.

In Figure 11, mirrors indicated by an N are in the entrance section that directs the beam of radiant energy into the stack. A tungsten filament bulb in a quartz envelope serves as the radiant energy source for wavelengths less than approximately 3.6 μm. Either a Nernst glower or an electrically heated nichrome wire covered with a ceramic material serves as a source for longer wavelengths. Two sources can be kept in place. Mirror N1 is removed or put in a place as shown, depending on the source being used. In normal operation, bypass mirrors B1, B2, and B3 are not in place. Mirror N2 forms an enlarged image of the source that overfills aperture Ap1; a further enlarged image of the source is formed on mirror N5, which directs the beam through a CaF_2 window into the stack. A field lens near aperture Ap1 images mirror N_2 on mirror N_3. A retroreflector described in the following paragraph, placed on the opposite side of the stack directs the beam back through the stack and forms another image of the source on mirror X1. Mirror X1 images mirror C3 of the retroreflector onto aperture Ap2 just ahead of the alternator. A rotating mirrored chopper A1, with two blades and two open sectors, alternately directs the beam through one of two paths. One alternate path contains correlation cell CC, and the other contains an attenuator. As discussed previously, the attenuator may be replaced by a high-pressure correlation cell. Mirror A5 directs the beam upward through a bandpass filter to the detector. Either of two liquid-nitrogen cooled detectors is used: PbS for $\lambda \leq 4$ μm, and PbSe for λ between 4 and 6 μm. The bandpass filter passes a spectral band that contains absorption by the gas being measured.

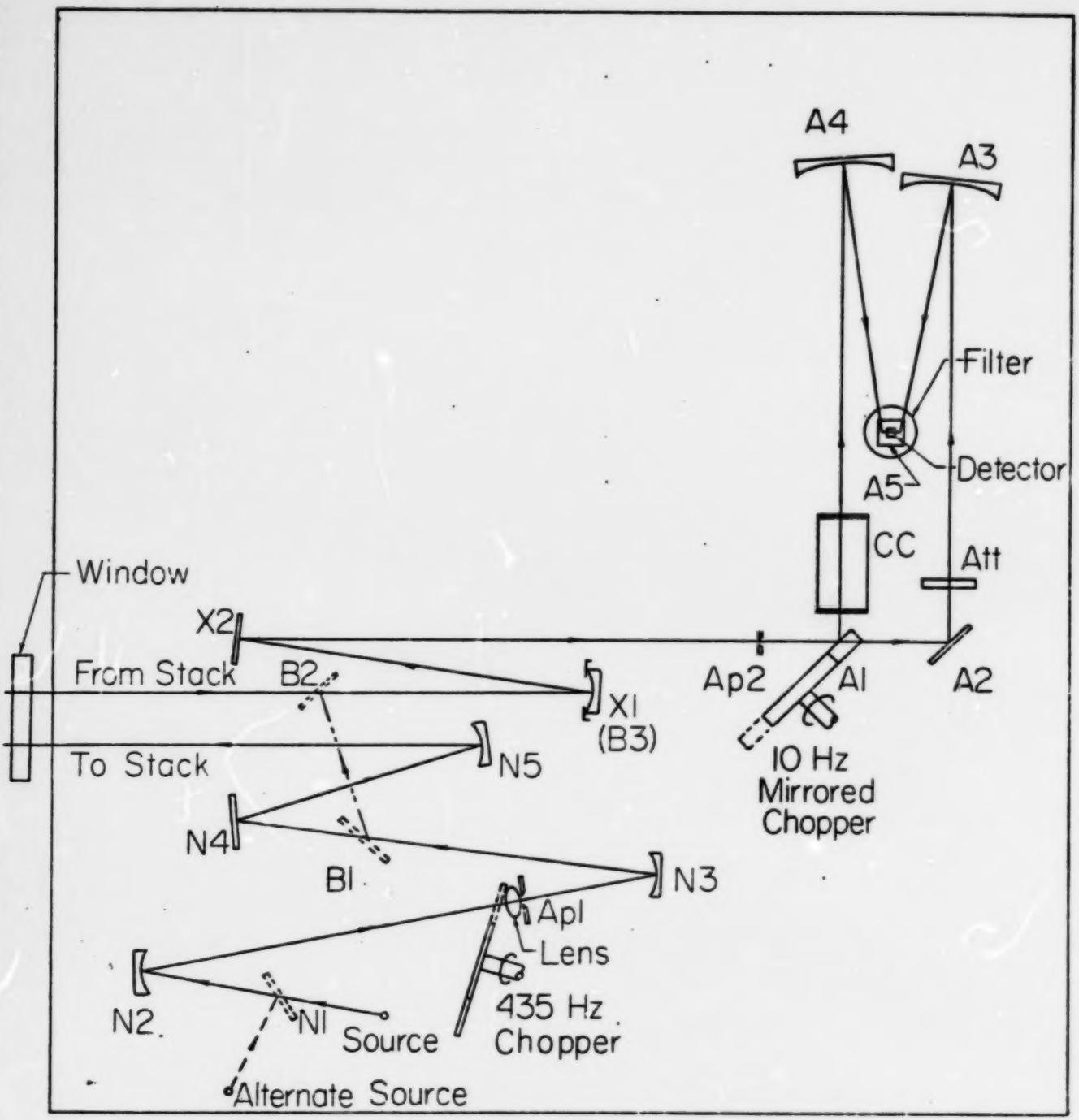

FIG. 11. Optical diagram of a gas-cell correlation instrument for across-the-stack measurements.

Figure 12 shows an optical diagram of the retroreflector assembly, which is a modified version of a "cat's eye" reflector. Mirror C1 forms an image of mirror N5 on the small spherical mirror C2, which is adjusted to correspond to the distance between C1 and N5. Mirror C2 images C1 near C3. Mirrors C1 and C3 are cut from a single spherical mirror and mounted so that their centers of curvature are at the same height but separated slightly in an azimuthal direction in order to image N5 on X1. Provided the relative positions of the three mirrors C1, C2, and C3 are rigidly fixed, the position of the image formed near mirror X1 relative to the effective source near N5 is insensitive to small angular or linear displacements of the retroreflector assembly.

The radii of curvature of the mirrors are chosen to be optimum for a stack approximately 3 m in diameter. For this size of stack, mirrors N2, N3, C1, and C3, aperture Ap2, and the detector are conjugate to each other. The source is conjugate to Ap1, N5, C2, and X1.

The instrument is very sensitive to differences in the energy passing through the two paths of the alternator section. Therefore, after the alternator has been balanced with no absorbing gas in the beam, it is very important that any changes in aperture or angular field of view affect both paths of the alternator in the same way. This is best accomplished by ensuring that the limits of the beam are well defined outside of the alternator and that the alternator transmit to the detector all of the beam entering it. The image of C3 at Ap2 is larger than the aperture, and the image of Ap2 at the detector is smaller than the sensitive element. Therefore, Ap2 forms the effective aperture as long as any misalignment of the optical components preceding it is sufficiently small that Ap2 remains completely filled. The windows and mirrors in the alternator section are oversized so that a mask in front of mirror X1 limits the angular field-of-view of the detector. The optical components preceding mirror X1 are designed so that the opening in the mask on mirror X1 is completely filled.

In order to balance the alternator, the bypass mirrors B1, B2, and B3 are easily positioned as indicated in Figure 11 to bypass the stack and provide an optical path with no absorbing gas. Bypass mirror B3 replaces X1, which has a different radius of curvature, and sits in the same position; the same mask is used for X1 and B3. When the bypass optics are in place, Ap2 is conjugate to mirrors N2 and N3 as it is when the beam is traversing the stack. Similarly, B3 is conjugate to the source and Ap1 as is X1 when it is in place. Thus, the instrument has the same field-of-view while it is being balanced as it has during a measurement. This method of bypassing the stack in order to balance the alternator matches the aperture and field-of-view about as well as is possible without passing the beam through the smokestack. Errors due to non-uniformities in the transmittance of stack windows or in the reflectivity of mirrors in the entrance section are minimized, but they cannot be eliminated completely. The best balance could probably be achieved by placing a pipe across the stack with the radiant energy beam passing through the pipe. The absorption could be eliminated by flushing the pipe with a non-absorbing gas. However, this method of balancing is frequently not practical because of space limitations or because of possible interference with the operation of the plant

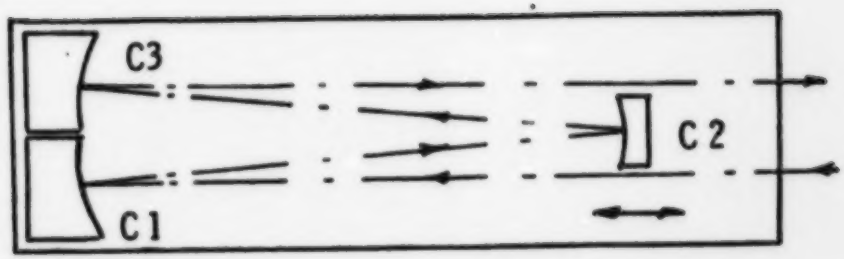

FIG. 12. Optical diagram of a retroreflector assembly used to redirect the radiant energy beam back across the stack to the gas-cell correlation instrument.

being monitored. It seems probable that the performance of gas-cell correlation instruments for stack measurements will ultimately be limited by the uncertainty in the balance corresponding to no absorption in the stack.

The radiant energy from the source incident upon the detector is chopped at 435 Hz with a 10 Hz modulation that is related to the concentration of the gas being measured. The detector signal is amplified and processed in such a way that the 435 Hz signal serves as a carrier for the 10 Hz signal as indicated by Figure 5. In this way, the system is insensitive to 10 Hz variations in the radiant energy on the detector unless the energy is first chopped at 435 Hz. Thus, emission by hot gases in the stack, or by any optical components that follow the 435 Hz chopper, does not influence the instrument output.

INSTRUMENT EMPLOYING GRATING ASSEMBLY

The stability and discrimination of an instrument of the type shown in Figure 11 could frequently be improved if the spectral bandpass could be controlled more accurately that can be done with an interference filter. Figure 13 shows another version of the instrument described above with a grating assembly to provide the desired bandpass. Either CO or NO can be studied with the grating assembly shown by blocking the beam at the appropriate retro-reflector R1 or R2. The bandpass filter near the detector eliminates overlapping orders of shorter wavelengths that are passed by the grating assembly. It is also necessary to change the correlation cell, and possibly the attenuator, when changing from one gas to another. A second grating assembly is built for SO_2 or HCl, and a third one serves for HF. Each grating assembly is constructed in its own box, and they can be interchanged quickly with little or no realignment of optical components required. The box for each assembly is mounted to the main base plate on a 3-point system that will not transfer stresses from the base plate to the box. All of the parts in the grating assembly are bonded in place with epoxy cement to avoid misalignment.

Mirrors T1, T2, and T3 are bonded to a block that can be removed or put back in place easily. This transfer optics assembly directs the beam into an entrance slit S1 that is below the optic axis of the alternator. The beams of the selected bandpass exits from the grating assembly through slit S2 at the height of the optics axis of the alternator. Mirror T3 directs the beam into the alternator. When the transfer optics are installed, it is necessary to tilt mirror X1 to direct the beam to the lower level of mirrors T1, T2, and slit S1. Otherwise, no adjustments are required when the transfer optics assembly is installed or removed.

Mirror T2 images mirror X1, and thus the source, on the entrance slit S1. For a stack diameter of 3 m, mirror C3 of the retroreflector is imaged on mirror T2. As the diameter changes with the resulting change in distance between mirrors C2 and X1, the conjugate to mirror C3 moves slightly from mirror T2. A mask on the grating limits the field-of-view of the detector.

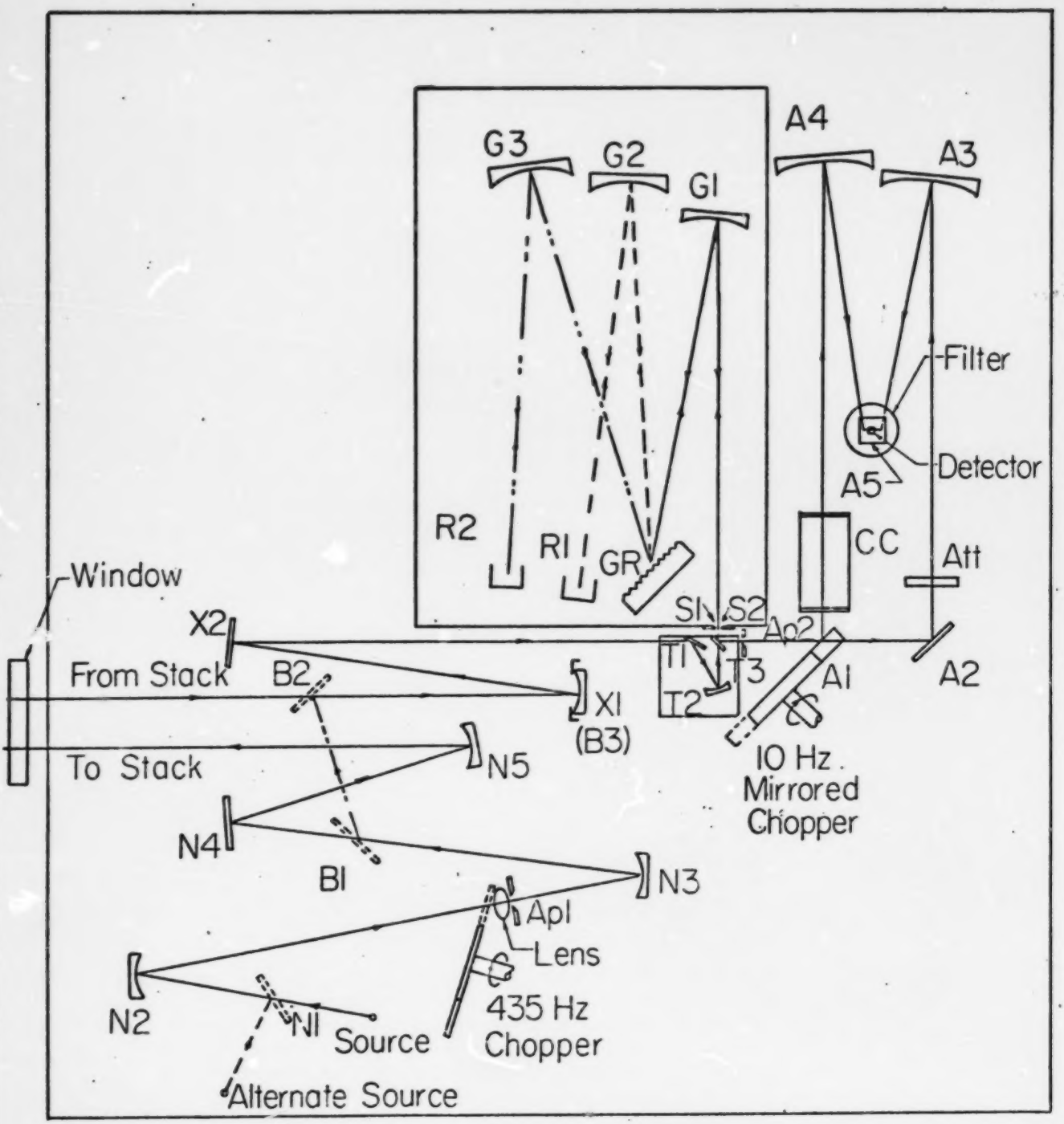

FIG. 13. Optical diagram of a gas-cell correlation instru[illegible]perating a grating assembly.

The grating assembly shown in Figure 13 disperses the radiant energy and directs that of wavelengths near 5.25 μm toward the retroreflector R1. Energy from a portion of the spectral band selected for the measurement of NO is redirected back to the grating, which undisperses it and directs it to mirror G1 and the exit slit S2. Similarly, wavelengths near 4.6 μm fall on retroreflector R2, which returns a portion selected to measure CO. Only one gas is measured at a time; the retroreflector not being used is covered with a mask.

A previous paper by one of us[6] describes the method by which the radiation is dispersed and a selected portion is undispersed and imaged. The original paper described the method for a prism as a dispersing element; however, the obvious application to a grating and to systems with a "tailored" bandpass were pointed out. Decker[7] has also described an application of the method to Hadamard spectroscopy.

A view of the retroreflector and grid assembly such as the ones indicated by R1 or R2 in Figure 13 is shown in Figure 14. A converging beam of dispersed radiant energy from mirror G2 (Figure 13) is incident upon mirror G4 whose reflecting plane is 45° from the vertical. The horizontal grid is in the focal plane where monochromatic energy forms an image of the entrance slit S1. Openings in the grid, such as the two shown in Figure 14, pass the selected spectral intervals to mirror G5. Mirrors G4 and G5 are normal to each other so that each ray of the beam returns to mirror G2 parallel to, but displaced vertically downward from, the ray before it struck mirror G4. The returning beam is completely undispersed by the grating, and the image formed at the exit slit S2 is undispersed and contains only those wavelengths passed by the grid in the retroreflector and grid assembly. Because an image of slit S1 is formed at slit S2, only one of these slits is required to provide the desired spectral resolution. Slit S2 is intentionally made somewhat wider than slit S1; the effective part of S2 is only that portion conjugate to the narrower S1. Slit S2 reduces scattered energy reaching the detector; having it oversize does not degrade the resolution and makes the positioning of the slits much less critical.

A photograph of the grating assembly for SO_2 and HCl is shown in Figure 15. A single mirror, G2, reflects the dispersed energy to both retroreflector and grid assemblies. Two separate mirrors cannot be used as G2 and G3 are for the NO and CO instrument shown in Figure 13. At mirror G2 of the grating assembly for SO_2 and HCl, the beams of dispersed energy for the two wavelengths of interest, 4.0 and 3.6 μm, overlap each other. The two beams near 5.2 and 4.6 μm used to measure NO and CO, respectively, are separated enough that two separate mirrors, G2 and G3, are used to focus the beams on the retroreflector and grid assemblies. By rotating G3 relative to G2, the two retroreflector and grid assemblies can be placed close to each other as shown in Figure 13. The grating assembly for HF contains a single retroreflector and grid assembly.

The power supply unit and the electronics unit shown in Figure 16 are designed for rack mounting and are connected to the optics assembly by approximately 15 meters of electrical cables. Power supplies and appropriate

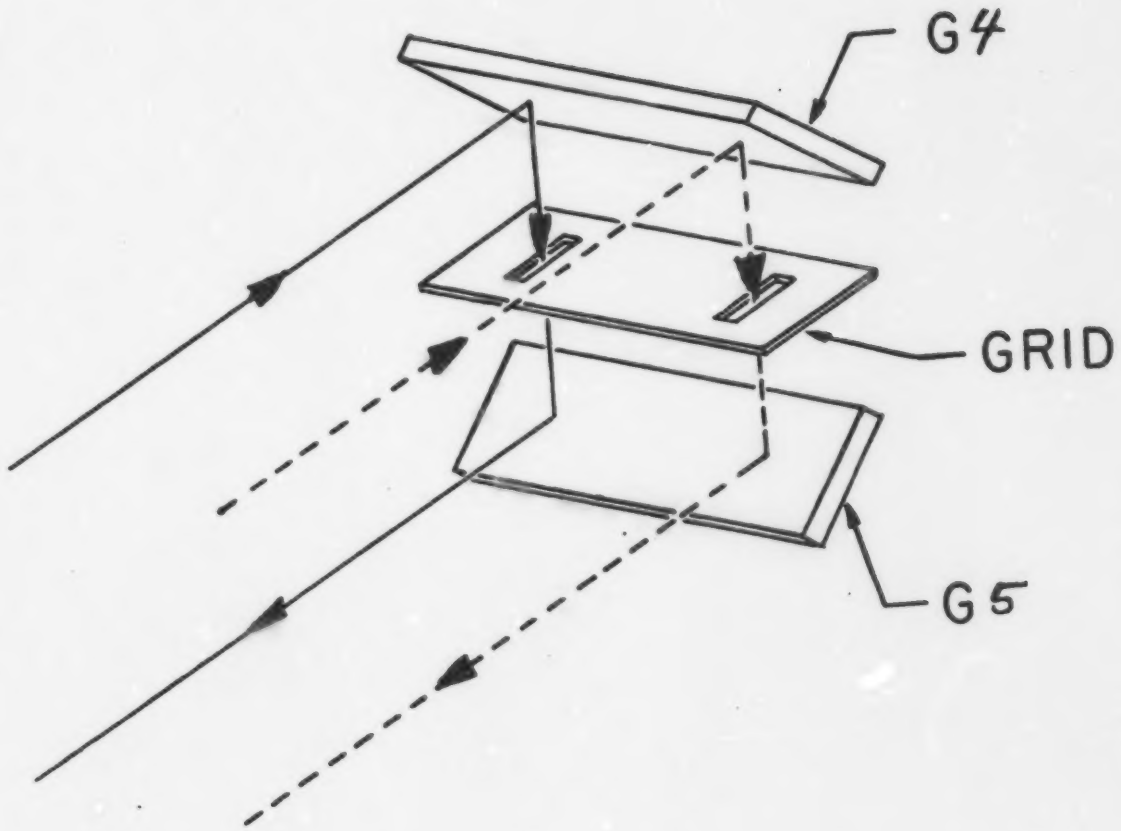

FIG. 14. Optical diagram of a retroreflector and grid assembly.

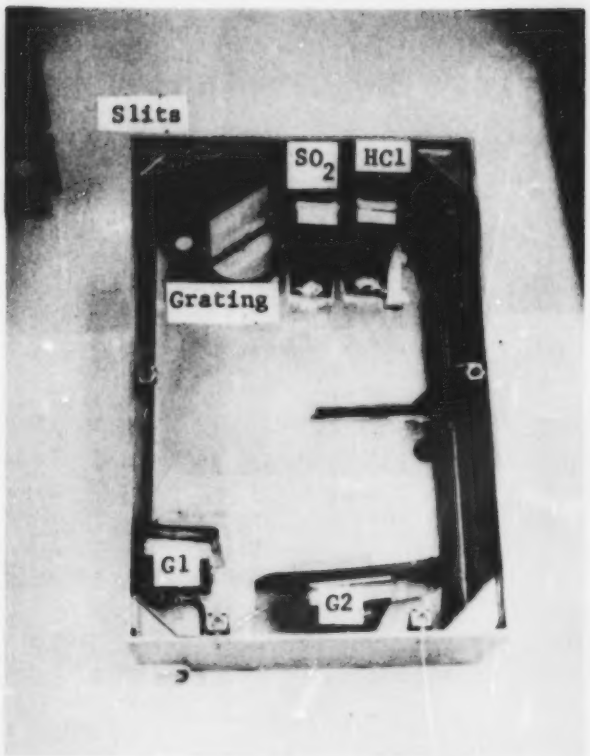

FIG. 15. The grating assembly for SO_2 and HCl. The two retroreflector and grid assemblies are labeled according to the gas they are used to measure.

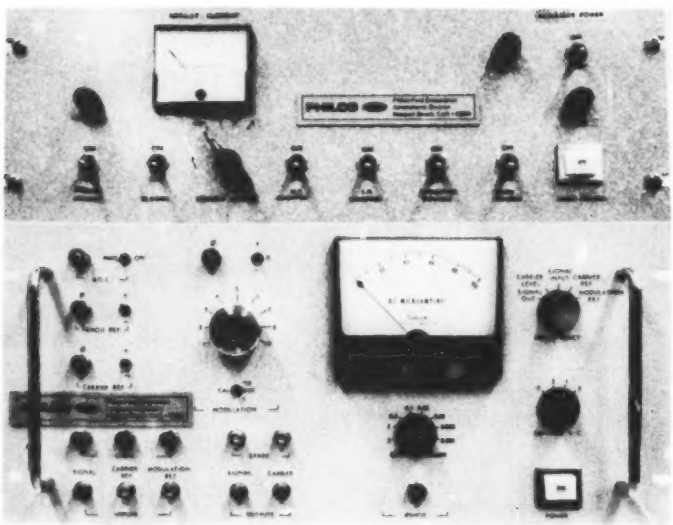

FIG. 16 The power supply unit above the electronics unit.

switches are provided for three different radiation sources: a Nernst glower, a nichrome-heated ceramic glower, and a tungsten-iodide bulb. Also included in the power supply unit are amperite ballast bulbs for the Nernst glower and a switch so that either 1, 2, or 3 of the ballasts can be connected in parallel to maintain a current of approximately 0.27, 0.54, or 0.80 amps. Motors for the two choppers and a heater to start the Nernst glower are also controlled from the power supply unit.

The amplified detector signal from the preamplifier on the optics assembly is fed into the electronics unit shown in Figure 16. All of the signal processing indicated by the electronics diagram of Figure 5 takes place in the electronics unit. Included on the front panel are gain controls and adjustments for the phases of the reference signals used in the synchronous demodulators. An electronic balance control, not shown in Figure 5, on the front panel of the electronics unit makes it possible to properly account for a possible small misbalance between the two beams in the alternator section when the stack is being by-passed to determine a "zero" reading.

By setting a switch to the appropriate position, the panel meter can be made to read either of five different voltages: signal input, carrier level, signal output, carrier reference, or modulation reference. The signal input represents the ac input at all frequencies and makes it possible to measure unwanted "pickup" when the chopped beam is blocked from the detector. The carrier level represents the signal at the output of the carrier-frequency demodulator. After the instrument has been properly calibrated, the absorber thickness of the gas being measured can be determined from the signal output, which can be read from the panel meter or from a recorder connected to an output jack. Nine different ranges exist for the signal output. The panel meter is also used when adjusting the levels of the carrier reference and the modulation reference signals. Time constants of 0.3, 1, and 3 seconds are available.

Two photographs of the optics assembly, with and without the cover, appear in Figure 17. The chopped radiant energy leaves the optics assembly before traversing the stack and returns from the stack through the open port in the front of the cover. The bracket directly beneath the opening in the cover fastens to a flange on the port of the stack. The detectors are filled with liquid nitrogen through an opening in the top of the cover; a cylindrical cap covers the opening and protects the detector. A small fan mounted above the source housing and visible in the lower photograph of Figure 17 circulates air and carries away much of the heat from the source. A preamplifier and a box for the bias battery are mounted on the baseplate near the front of the instrument and adjacent to the grating assembly.

SPECTRAL PROPERTIES OF THE GASES

Figure 18 shows two experimental curves of transmittance in the region of the Q-branch and the R-branch of the fundamental NO band. The absorption represented by the upper curve is due to approximately 1.5% H_2O in 8 m of

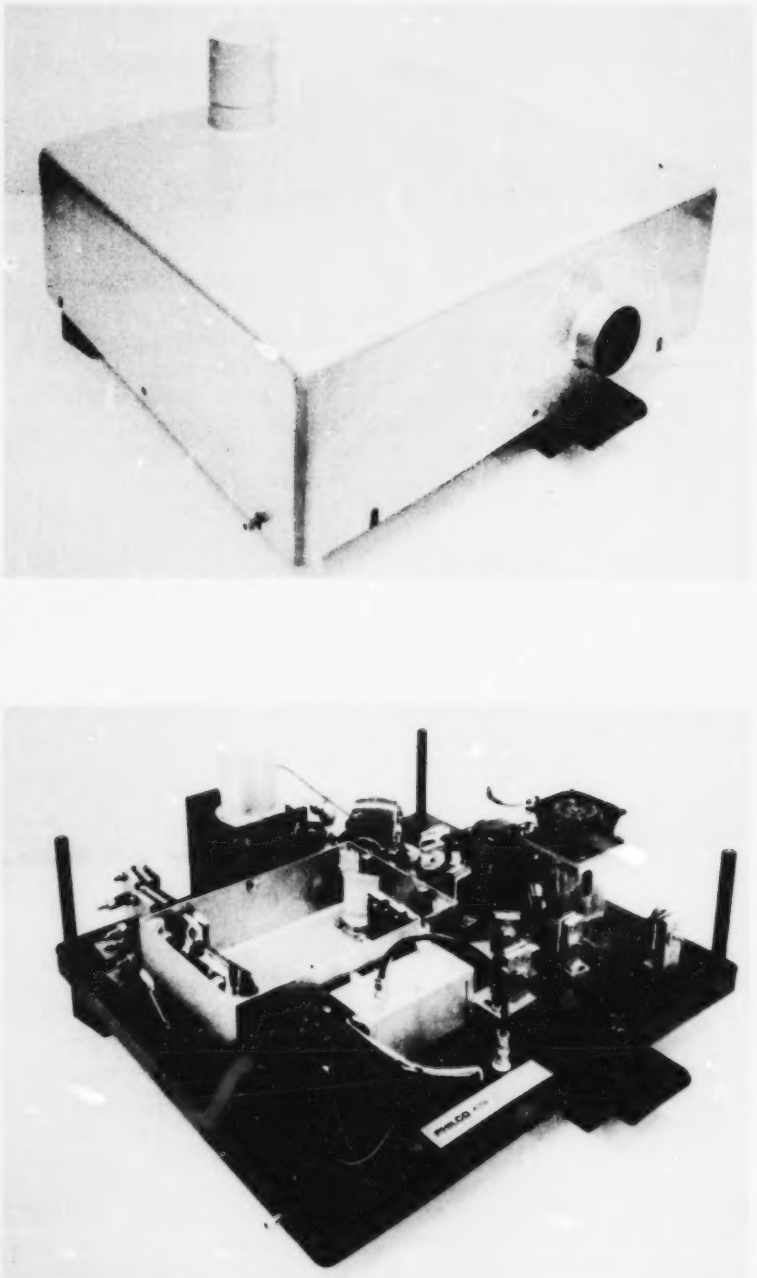

FIG. 17. Photographs of the optical assembly. The top picture shows the assembly with the cover installed.

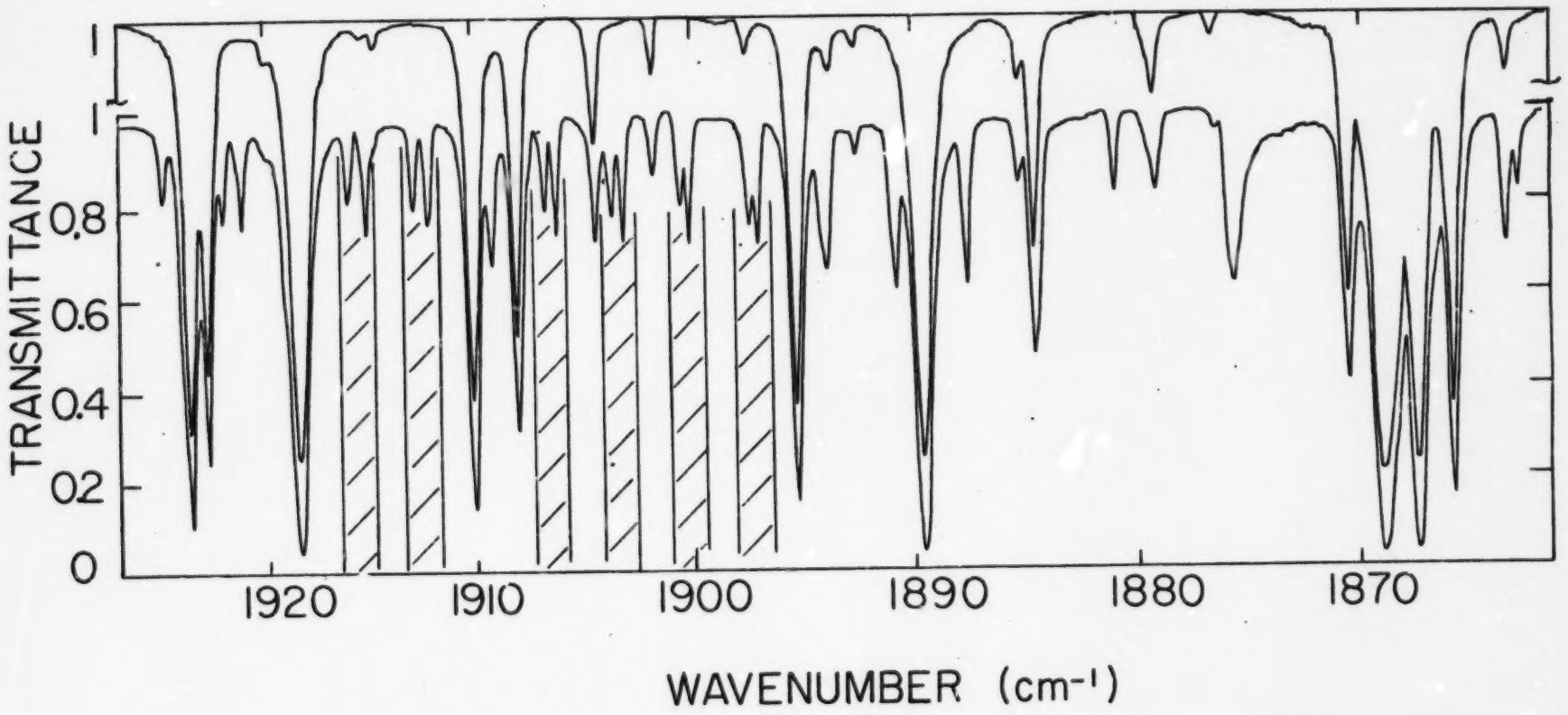

FIG. 18. Spectral curves of transmittance of H_2O and of H_2O + NO between 1862 and 1928 cm^{-1}. Spectral slit-width = 0.35 cm^{-1}. The transmittance scales of the two curves differ by 0.20.

room air. The lower curve, which is displaced downward for clarity, represents the same amount of H_2O and a sample of 0.03 atm of NO in a 10 cm sample cell. The need to reduce interference by H_2O is apparent. Absorption by H_2O is even stronger in the lower-wavenumber P-branch of the NO band. The cross-hatch areas correspond to the 6 narrow spectral intervals passed by the retroreflector and grid assembly for NO. Interference by H_2O is reduced by choosing the intervals with a minimum of H_2O absorption. Each interval contains a pair of NO lines.

Blocking the spectral intervals where there is little or no NO absorption decreases Σ with essentially no decrease in Δ. (See Equations 3 and 4.) Thus, the Pembrook Factor F is increased with a resulting increase in the stability of the zero balance. The blocked energy, if allowed to pass, would provide no information about NO concentration, but it would add to any misbalance of the alternator. Information on the positions, intensities, and half-widths of the NO lines can be obtained from two articles by Abels and Shaw.[8,9]

Two transmittance curves of the SO_2 band employed are shown in Figure 19. The structure in Curve A is due to "clusters" of many closely-spaced lines that are not resolved. When the total pressure of the sample is greater than about 1 atm, the lines are broadened enough that they overlap considerably and much of the structure in a spectrum of 1 atm sample that could be observed with a very narrow spectral slitwidth is not greatly different from Curve A. Further smoothing of the spectrum with increased pressure is illustrated by Curve B of Figure 19. At the high pressure, the widths of the SO_2 lines are comparable to the spacings between the clusters of lines.

The relatively "shallow" structure in the spectrum of SO_2 near 1 atm contributes little to the sensitivity of a gas cell correlation instrument for thisgas when the sample is near 1 atm, as in a smokestack. The greatest sensitivity can be achieved by making use of the coarse, deep structure. In order to do this, the grid for SO_2 has been made with only two openings that pass two spectral intervals, each about 4.7 cm^{-1} wide. One is centered in the region of strong absorption near 2513 cm^{-1}, and the other is centered outside the region of significant absorption near 2538 cm^{-1}.

Enough SO_2 is contained in the correlation cell that it is essentially opaque in the 2513 cm^{-1} interval while it is nearly transparent in the other interval. It follows from the previous discussions on the spectroscopic principles that the transmittance of the attenuator is approximately 50% over both spectral intervals. The amount of radiant energy passing through the correlation cell is only very slightly dependent on the amount of SO_2 in the sampling region. When the attenuator is in the beam, the SO_2 in the sampling section absorbs in one of the two spectral intervals passed to the detector. Approximately twice the contrast in the two beams of the alternator could be achieved if the alternator transmitted only in one of the two intervals during one-half of each cycle and only in the other interval during the other half. Because of the relatively wide spectral intervals involved, 4.7 cm^{-1}, it would not be difficult to accomplish this by modulating the energy with a chopper in the plane of the dispersed energy in the grating

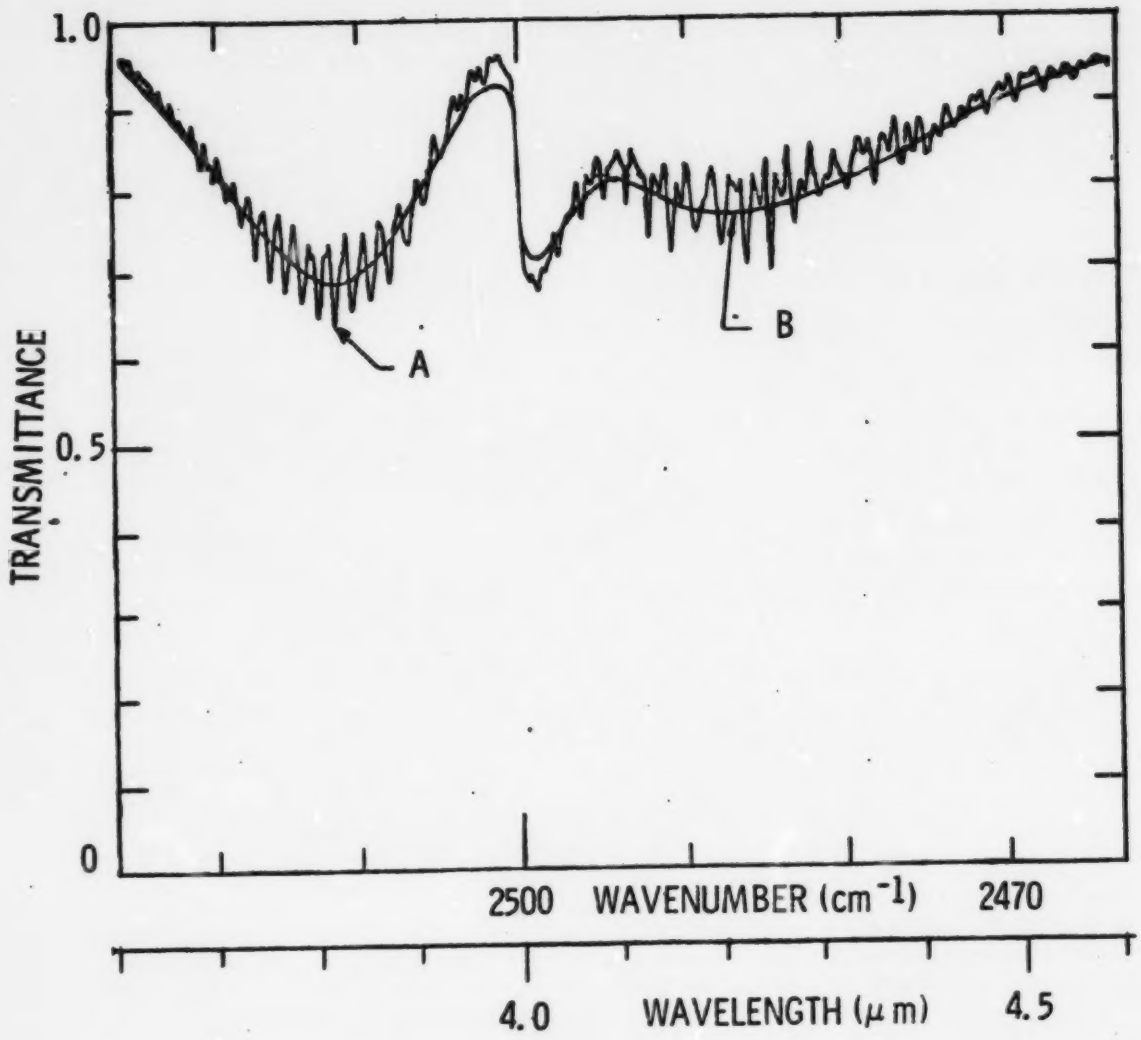

FIG. 19. Spectral curves of transmittance between 2465 and 2525 cm^{-1}. The total pressures of the two dilute, room-temperature, mixtures of SO_2 in N_2 are 1.00 atm for Sample A and 15.0 atm for Sample B. u = 0.78 atm cm for Sample A; u for Sample B was reduced a few percent to produce nearly the same average transmittance as Sample A. The spectral slitwidth $\cong$ 0.35 cm^{-1}.

assembly. In this case a correlation cell would not be required. Alternating between two similar intervals could also be done with narrow-bandpass filters. It follows from the above discussion that gas-cell correlation methods do not provide the advantages in terms of effectively high spectral resolution for SO_2 that they do for other gases such as HCl, HF, NO, CO, or CO_2 whose spectra consist of distinct, well-separated lines.

Two bands of SO_2 centered near 1150 cm^{-1} and 1360 cm^{-1} are stronger and would provide higher sensitivity than the one used. However, H_2O interference is much more troublesome and detectors are less sensitive in the regions of the two lower-wavenumber bands. Data on the absorption by these bands are given in Reference 10.

Data on the absorption properties of CO, HCl, and HF are available in a number of reports and papers. Line parameters used in the design of the present instrument are from Benedict, et al[11] for CO; Benedict, et al[12] for HCl; Meredith and Kent[13] and Herget, et al[14] for HF.

LABORATORY TESTS AND CALIBRATION DATA

Figures 20, 21, and 22 show plots of $V' = V_a/V_c$ for each of the 5 gases with the appropriate grating assembly in place as indicated by Figure 13. These curves can be used for calibration to convert the instrument output to the partial pressure p of the gas species being measured. The ordinate for each of the figures corresponds to the ratio Δ/Σ plotted in Figure 8, and the abscissa is the absorber thickness of the gas normalized to room temperature, 296 K. The curves for CO and NO in Figure 20 are based on samples at 296 K, and $u = p\ell$, where p is the partial pressure of the absorbing gas in atm and ℓ is the geometrical path length in cm. All of the samples used to obtain the data contained the absorbing gas mixed with N_2 at 1 atm total pressure.

Samples of CO + N_2 and NO + N_2 were also investigated at approximately 420 K (279°F) which is typical of smokestack exhaust. We found that a single curve can be used if the value of u is normalized to 296 K by

$$u(\text{atm cm}_{296}) = \frac{P(\text{atm})\ell\ (\text{cm})\ 296}{\theta}\ , \text{ or } p = \frac{u\theta}{296\ \ell}\ ,$$

where θ is the stack temperature. By normalizing in this manner, the systematic error introduced by using a single curve is not more than approximately 5% over the temperature range investigated. The validity of this simple expression for normalizing indicates that the absorption is nearly independent of temperature changes provided the number of molecules in unit cross-sectional area of the beam remains constant.

The SO_2 data obtained at the two different temperatures cannot be represented by a single curve. Thus, accounting for the stack temperature is somewhat more complicated for SO_2 than for CO or NO. Concentrations of SO_2 could be determined graphically from the two curves of Figure 21 by interpolation

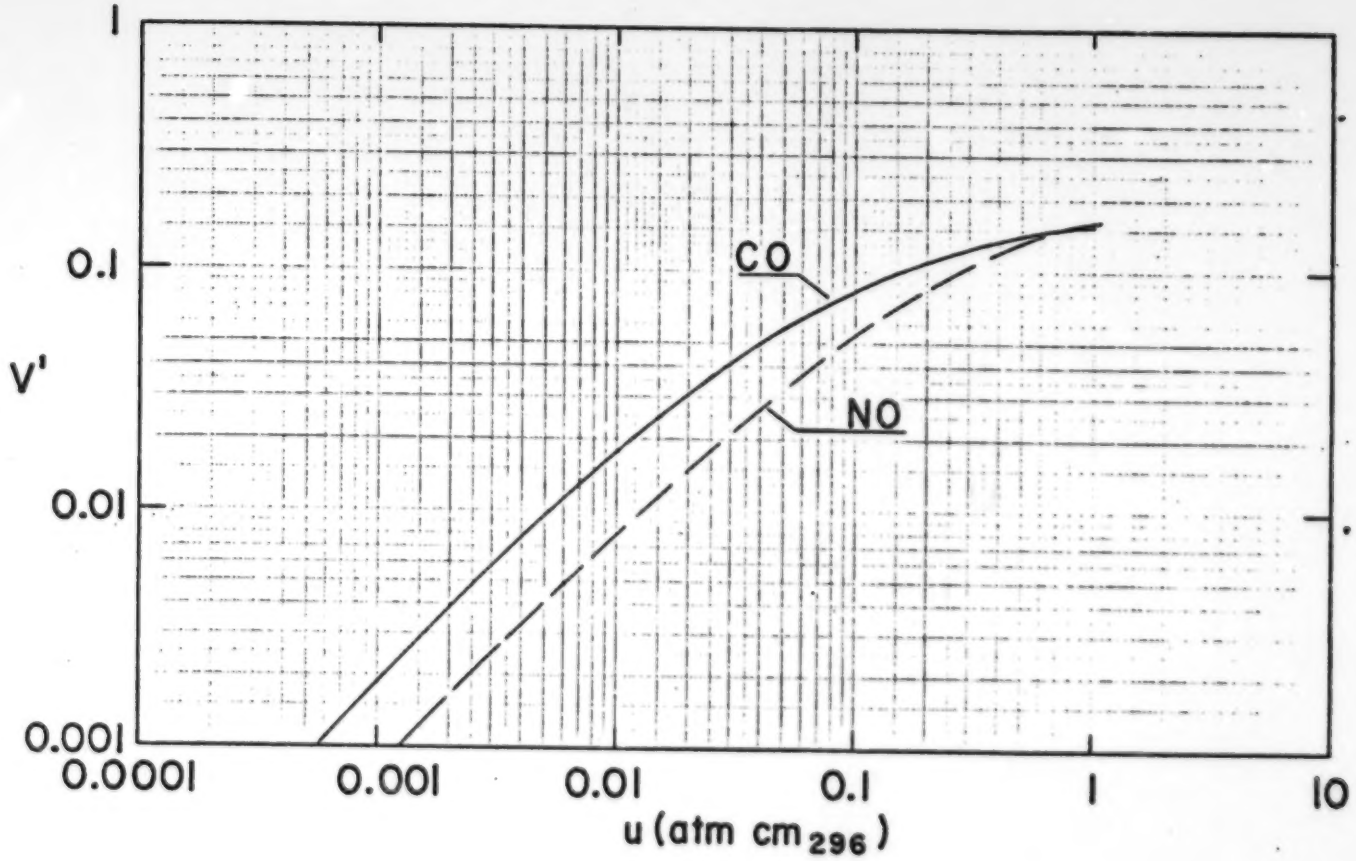

FIG. 20. Curves of V' versus normalized absorber thickness for CO and NO. The correlation cell parameters are: p = 0.461 atm, L = 2 cm for CO; and p = 0.414 atm, L = 2 cm for NO.

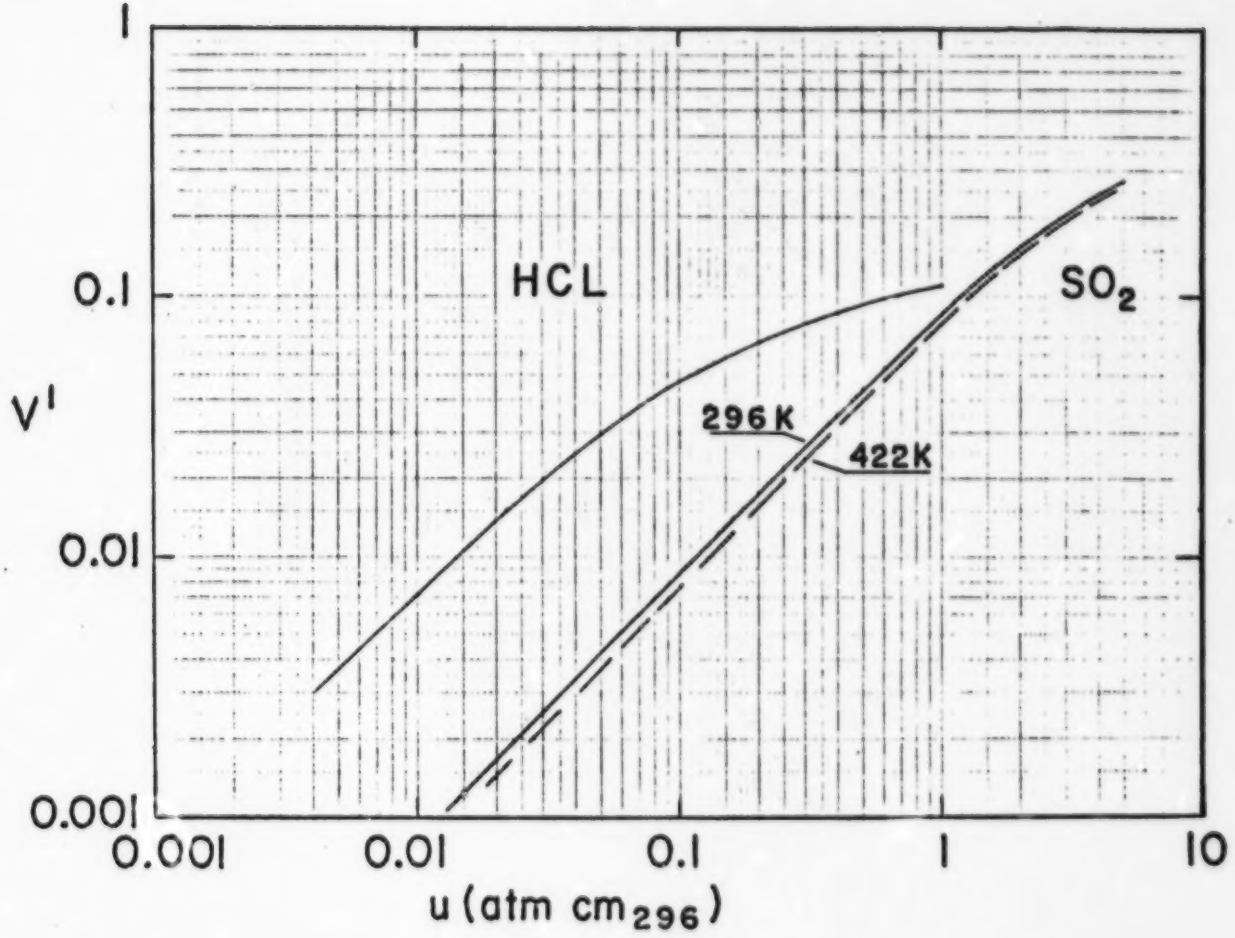

FIG. 21. Curves of V' vs normalized absorber thickness for SO_2 and HCl. The results for the elevated temperature 422 K for SO_2 are shown as a broken curve. The correlation cell parameters are: p = 0.539 atm, L = 1 cm for HCl; and p = 2 atm, L = 5 cm for SO_2.

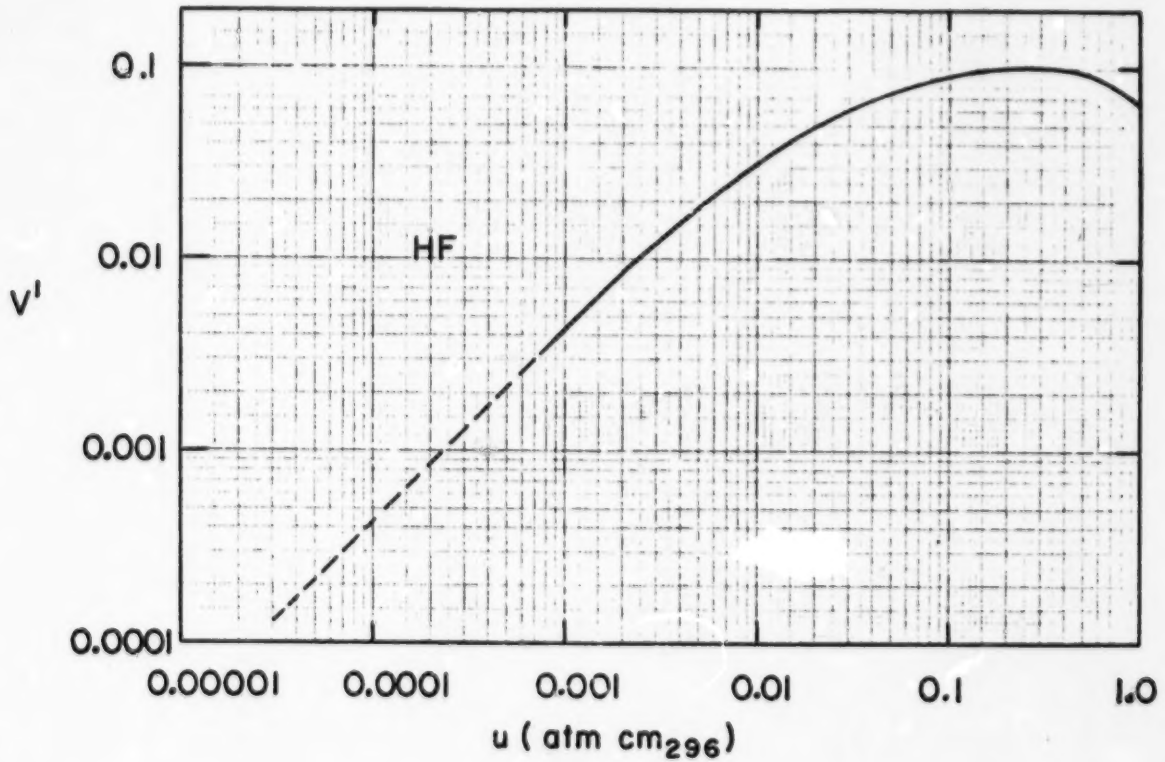

FIG. 22. Curve of V' vs normalized absorber thickness for HF. The solid portion is based on laboratory data, the dashed portion on calculations. The correlation cell parameters are p = 0.164 atm, L = 1 cm.

for temperatures between 296 K and 422 K. The temperature can also be accounted for empirically by use of the follwoing expression:

$$p = \frac{u(\text{atm cm}_{296})\ \theta}{296\ \ell} = \frac{\theta\ u'}{296\ \ell}\ \left[1 + 0.001\ (\theta - 296)\right]. \qquad (8)$$

The uncorrected value of u' is determined from V' and the solid SO_2 curve of Figure 21.

No calibration data were obtained for HCl or HF at other than room temperature. For elevated temperatures less than approximately 420 K, it is probably safe to account for temperature in the simple manner used for CO and NO.

Table 2 summarizes the important parameters and the performance of the instrument for the 5 gases of interest when the appropriate grating assembly is being employed. The second column lists the spectral intervals passed by the grid in the retroreflector and grid assembly. As indicated in the discussion of Eq. (6), the Pembrook Factor given in the third column relates the absorber thickness of the gas in the sample to the resulting percentage misbalance in the two alternator beams.

A Nernst glower source heated by 0.8 amp of alternating current was used in measuring the absorber thickness required to produce a signal equivalent to the peak-to-peak noise arising from the detector. A 3-second time constant was employed. The laboratory optical path simulated a double-passed stack 3 m in diameter with 5 cm diameter windows. Both the PbSe and PbS detectors have 2 mm x 2 mm sensitive elements cooled with liquid nitrogen.

Water vapor produces the most serious interference when measuring NO. The discrimination ratio (10,000:1) is based on a 3 m diameter stack containing 5% H_2O. Because of a non-linear relationship between the H_2O absorber thickness and the instrument response, the discrimination ratio depends on the amount of H_2O. Unrealistically high discrimination ratios can be observed with high concentrations of the interfering gas. A meaningful discrimination ratio should be measured with approximately the same absorber thickness of the interfering gas as will be encountered during a measurement.

Several measurements of H_2O interference were made while measuring NO with a different instrument employing various bandpasses that included several of the H_2O lines seen in Figure 18. Typically, the H_2O interference was 10-100 times as great as that observed with the grating assembly with a bandpass of 6 narrow spectral intervals. By employing the grating assemblies to carefully select the bandpasses, it has been possible to reduce the interference by other gases to a negligible amount while measuring CO, SO_2, HCl, or HF.

Hydrogen fluoride is highly reactive, and it adsorbs and desorbs on and off of the walls of the gas-handling system and correlation cell. Therefore, concentrations of the dilute HF mixture were difficult to determine accurately. Samples of HF concentration between 0.1% and 1% were prepared in a 1 cm sample cell in the following manner to provide calibration sample absorber thicknesses between approximately 0.001 and 0.01 atm cm_{296}. A stainless steel cylinder was used to make a 1% HF mixture in N_2. The cylinder was preconditioned for adsorption by introducing pure HF into the cylinder at a slightly higher pressure than would be used in the mixture and allowing the gas to react with the walls for approximately one hour. The HF was pumped out and the desired 1% HF in N_2 mixture made.

The cylinder was attached to the sample cell with a short piece of tubing to reduce adsorption in the lines. In order to obtain samples with concentrations below 1%, the sample cell was filled with the 1% mixture to a predetermined pressure, always less than 1 atm. The total pressure in the sample cell was then increased to 1 atm by adding N_2. This method gave consistent results for concentrations as low as approximately 0.1%. At lower concentrations, apparent variations in the amount of adsorption and desorption made the results unreliable. A shorter sample cell was not available to enable us to make samples of smaller absorber thickness while maintaining an accurately measurable concentration.

In order to extend the calibration curve to smaller values of absorber thickness, we employed published values for the HF absorption line parameters to calculate the expected instrument response. The calculations also involved the spectral bandpass, the amount of HF in the correlation cell, and use of the Ladenberg-Reiche function[15] for absorption by a spectral line. For very small absorber thicknesses, V' is proportional to u, as is indicated by the broken line of unity slope in Fig. 22. The calculated values agreed with the experimental values for u between approximately 0.001 and 0.005 atm cm_{296}.

We have used this calculation method previously for other gases whose line parameters are well-known. Generally, the shape of the curve can be calculated quite accurately for values of u up to where the slope of a calibration curve such as the one in Fig. 22 has decreased to about 0.5. The calculated curve of V' vs u may require a slight shift up or down to match an experimental curve, but the shapes of the two curves on log-log scales are nearly identical. Because of our previous success in calculating calibration curves, and because of the agreement between the calculated and measured values for several values of u, we believe that both the solid and dashed portions of the calibration curve in Fig. 22 are accurate to less than $\pm$ 10%.

When measuring HF, the discrimination against H_2O is 50,000 : 1. Most of the interference by H_2O is due to the longest wavelength interval which is passed by the grid slit nearest the grating. If more discrimination against H_2O is needed, the grid slit that passes the longest wavelength could be blocked and only the other two grid slits used. New HF calibration data would have to be obtained for the assembly used in this fashion.

TABLE 2

INSTRUMENT PARAMETERS AND PERFORMANCE

Gas to be Measured	Spectral Band Pass	Pembrook Factor^{-1} (atm cm)	Detector and Noise-Equivalent Absorber Thickness (atm cm)		Remarks on Interfering Gases
NO	6 intervals, each centered on a pair of NO lines near 1900 cm^{-1}.	0.81	PbSe 0.003	H_2O	D.R. = 10,000:1 with H_2O at 125°C. 5% H_2O produces error corresponding to 5 ppm NO. The 6 pairs of NO lines in the spectral bandpass are relatively free of H_2O absorption. Inclusion of other lines would increase the interference by H_2O.
CO	11 intervals, each centered on a CO line between 2150 and 2200 cm^{-1}.	1.85	PbSe 0.0008	CO_2	Interference too small to measure. D.R. > 200,000:1 with CO_2 at 125°C. 10% CO_2 produces error corresponding to less than 0.5 ppm CO
				H_2O	D.R. ≃ - 50,000:1 with H_2O at 125°C. 5% H_2O produces error corresponding to -1 ppm CO.
SO_2	2 intervals, near 2538 and 2513 cm^{-1}.	0.088	PbS 0.011		No significant interference by other gases in stacks of coal-burning plants in this spectral region.
HCl	4 intervals, each includes corresponding lines of 35_C and 38_C isotopes. Intervals are between 2750 and 2850 cm^{-1}.	0.7	PbS 0.003		Intervals in the spectral bandpass are essentially free of interfering absorption. H_2O absorbs near the adjacent lines. SO_3 might interfere with one of the HCl lines.
HF	3 intervals, each passes a line between 3995 and 4080 cm^{-1}.	4.2	PbS 0.0001		D.R. ≃ 50,000:1 with H_2O at 150°C. Improved discrimination can be obtained by blocking the long wavelength grid slit.

No data have been obtained with the instrument shown schematically in Figure 11 without the grating assembly. However, from other data obtained in our laboratory with instruments employing narrow bandpass filters in the place of a grating assembly, we can conclude that the simpler filter instrument provides a higher ratio of signal to detector noise at the expense of poorer discrimination and a lower Pembrook Factor.

FIELD TESTS

Field tests of the instrument measuring NO, CO, and SO_2 were performed on a smokestack of a coal-burning power plant in Charlotte, N.C. Photographs of the optics assembly and retroreflector mounted on the stack are shown in Figure 23; the cover of the optics assembly has been removed. The side of the optics assembly next to the stack is connected by a hinge to a flange welded on the stack. Two adjustable legs support the back side of the optics assembly; the legs can be adapted to a variety of stacks.

Two ports with 10 cm openings are welded permanently on opposite sides of the stack at approximately 1.5 meters above the level of the flat roof. The effluent temperature was approximately 422°K (300°F). The two-way optical path length through the effluent was approximately 580 cm. A small building approximately 6 meters from the stack housed the power supply unit and the electronics unit.

A CaF_2 window is mounted on a shutter to prevent stack effluent from escaping into the instrument. Compressed air blown over the inside surface of the window prevents the accumulation of dirt on the window. The air then passes into the stack through a cylindrical tubing that extends approximately 30 cm into the stack. Because of the air flow through the tubing, very little effluent reaches the window. Although the required air flow was greater than expected, the windows remained clean enough for operation for several hours. The window is mounted on a sliding shutter that can be closed easily to protect the window when the instrument is not in use. A similar window arrangement with plumbing for compressed air is mounted on the retroreflector assembly on the side of the stack opposite the optics assembly.

Smoothed plots of the NO concentration measured at four different times are shown in Figure 24. During three of the four periods, measurements were compared with valves obtained with a DuPont Model 460-1 analyzer. We note that the data obtained with the two instruments agree quite well. The DuPont instrument extracts a portion of the effluent from the stack and employs the uv to measure the NO_2 concentration. The NO is then oxidized to NO_2, and another NO_2 measurement is made. From the difference between the NO_2 concentrations, the original NO concentration in the effluent can be determined. The NO_2 concentration in the effluent before it leaves the stack is generally much lower than that of the NO.

Similar smoothed plots of the CO concentration are shown in Figure 25. The relatively low concentration varying between 5 ppm and 20 ppm indicates that the combustion was nearly complete. Simultaneous measurements made with an extractive NDIR CO analyser resulted in average values near 9.5 ppm during

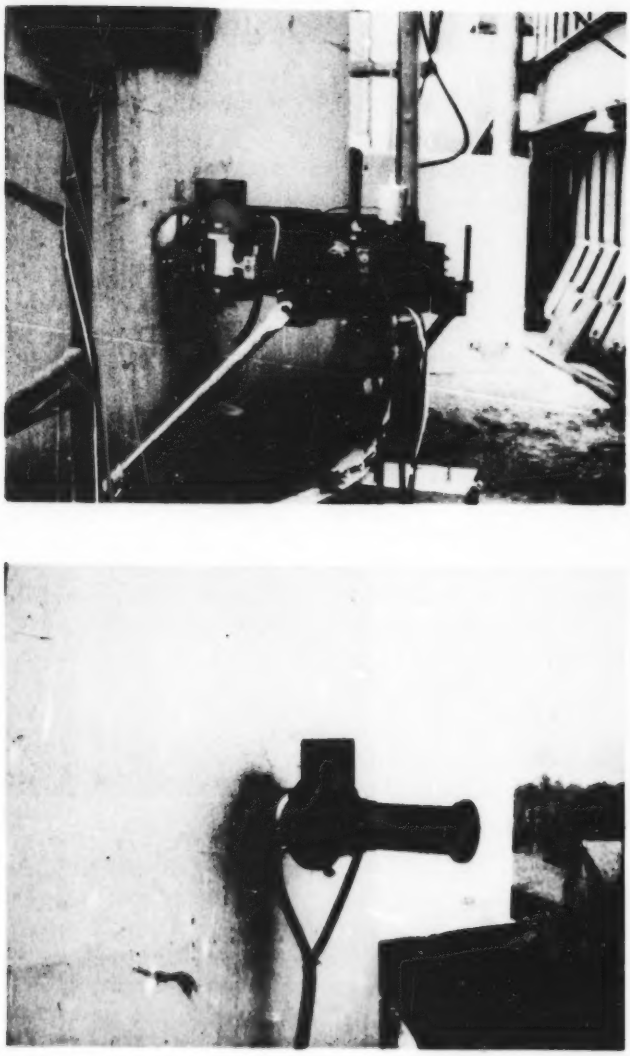

FIG. 23. The optics assembly and the retro-reflector mounted on the smokestack of the Duke Power Co. at Charlotte, N. C.

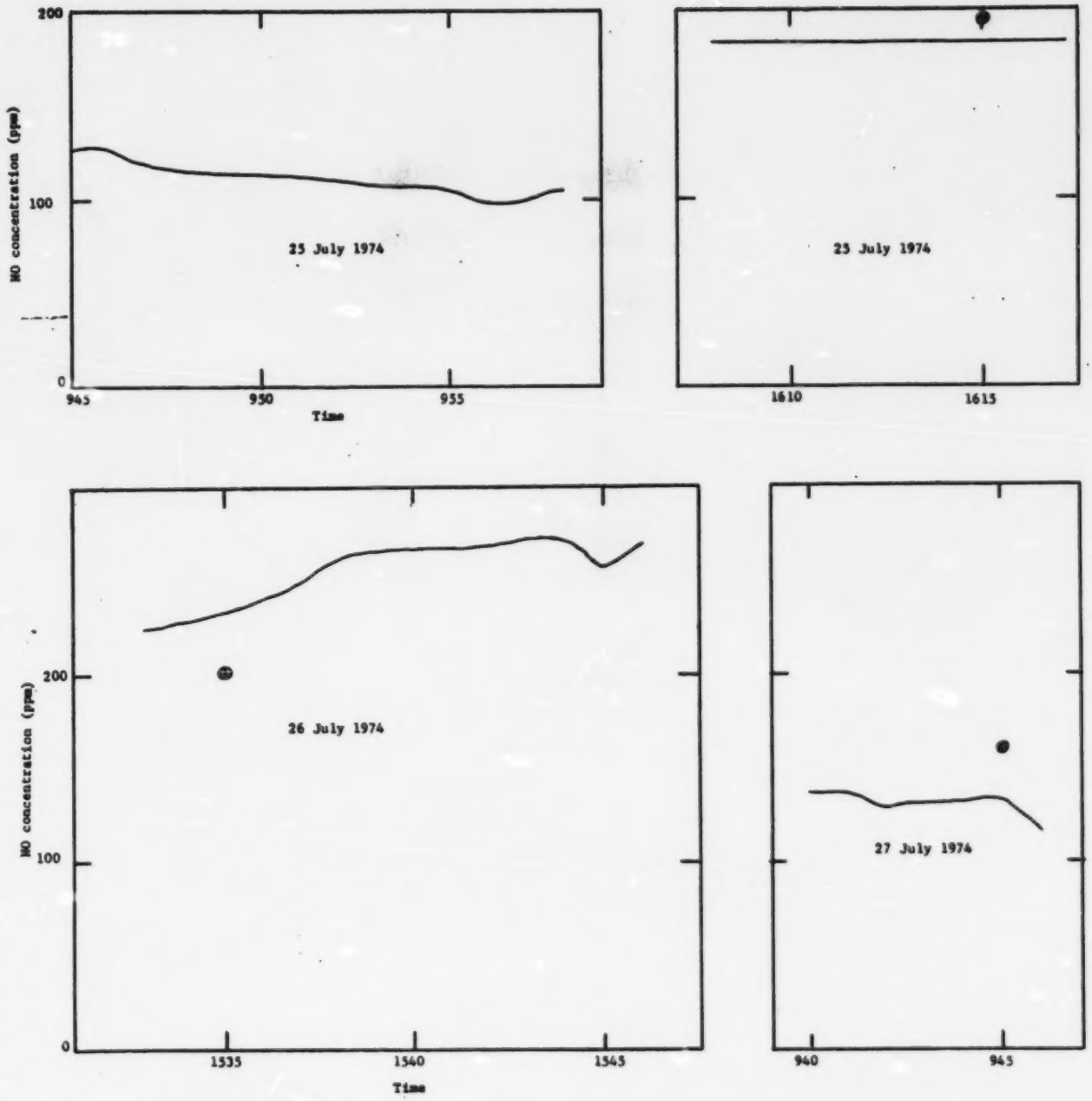

FIG. 24. Plots of NO concentration vs time for 3 different days at the Duke Power Co., Charlotte, N.C. The peak-to-peak noise was 14 ppm. The symbol ⊕ represents the data obtained with a DuPont Model 460-1 analyzer.

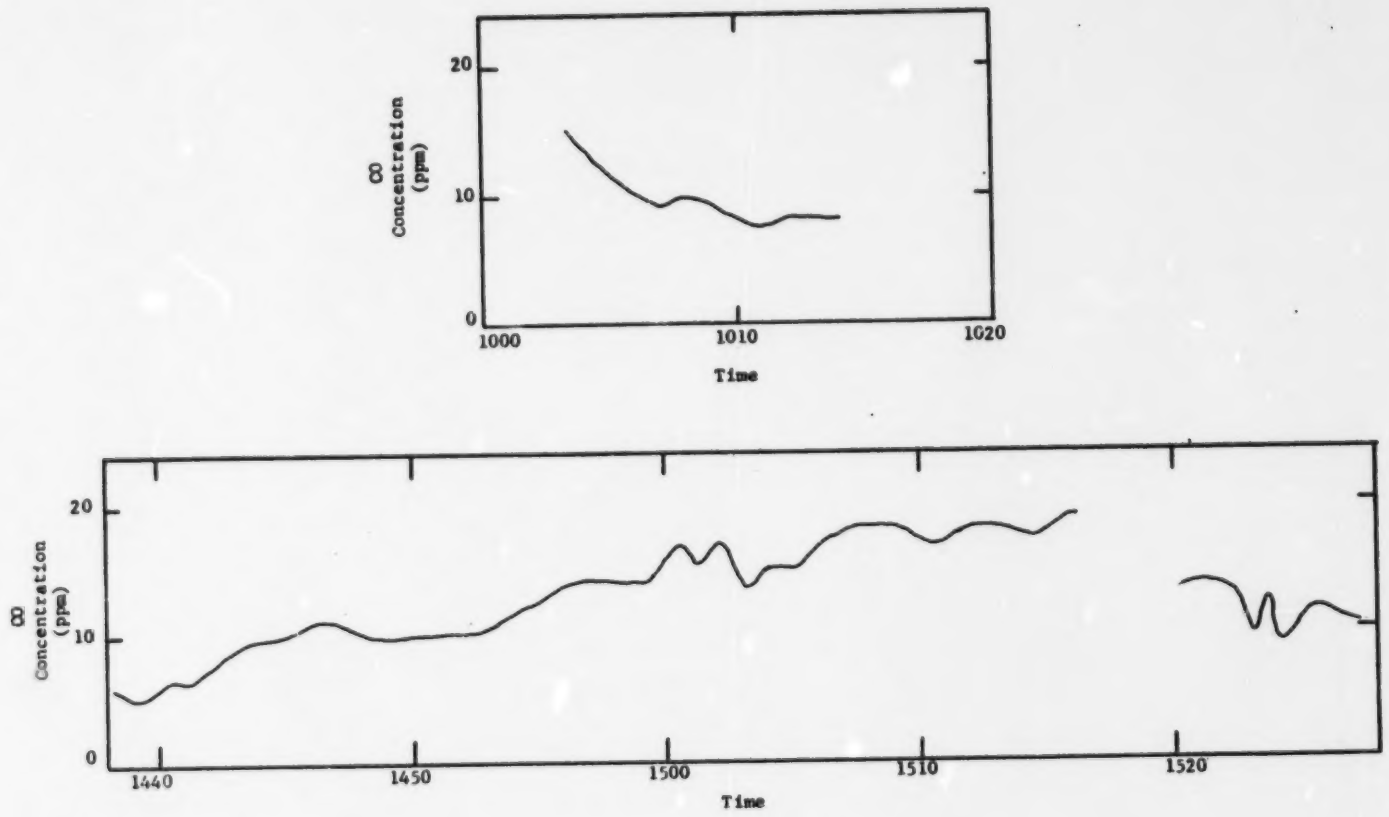

FIG. 25 Plot of CO concentration vs time of day for 25 June 1974 at Duke Power Co., Charlotte, N. C. The peak-to-peak noise was 2.8 ppm.

the 3 day period of 25, 26 and 27 June 1974. Several months earlier we had employed a small grating spectrometer to scan transmission spectra of the same stack. From these spectra we estimated the average CO concentration to be 15 ppm.

Data on the SO_2 concentration are shown in Figure 26 for periods during three different days. Agreement with the data by the DuPont instrument is good. Effluent was extracted from the stack by the DuPont instrument and uv spectroscopic methods were employed to determine the SO_2 concentration. During the beginning of the period of measurement on 26 June 1974, both instruments indicated essentially the same concentration. After about 9:10, the DuPont instrument indicated a nearly constant concentration while the Philco-Ford instrument indicated that the SO_2 concentration was decreasing slowly. No satisfactory explanation for the difference is given.

The high level of noise observed while measuring SO_2 was due to the PbSe detector being used. Ordinarily a liquid-nitrogen cooled PbS detector is used for SO_2; however, the dewar for this detector had lost its vacuum and could not be used. The detectivity of the PbS detector is only about one-tenth that of the PbSe detector at 4 μm.

The noise-equivalent concentration of NO and CO were both approximately twice as high as would be expected on the basis of the laboratory data represented in Table 2. For example, the noise-equivalent absorber thickness of 0.003 (atm cm_{296}) of NO corresponds to approximately 7 ppm for the 5.80 meter two-way path across the stack at 422 K. Any one of several factors may have attributed to the lower signal-to-noise ratios observed in the field: dirt on the windows, turbulence and vibration, or improper alignment. Exposure of the detector to sunlight during the alignment also probably increased the detector noise for several hours after the exposure. This latter factor seems quite probable since the detector did appear to behave abnormally for a while after it had been exposed to the sun.

No field tests have been made for HCl or HF to date, although such tests are planned by EPA personnel in the near future.

In general, the instrument performed quite satisfactorily during the field tests. The sensitivity, detectivity, and discrimination against interference by other gases are more than adequate for most applications. As indicated previously, the largest contribution to the measurement errors probably comes from uncertainty in the zero setting. A few minor problems were encountered, but these can be remedied easily. Among these were the accumulation of dirt on the windows, binding of the window shutters, and difficulties in changing the detector, or refilling it with liquid nitrogen, without exposing it to the sunlight.

It is anticipated that additional tests performed with this versatile instrument will provide information that is helpful in the design of simpler gas-cell instruments.

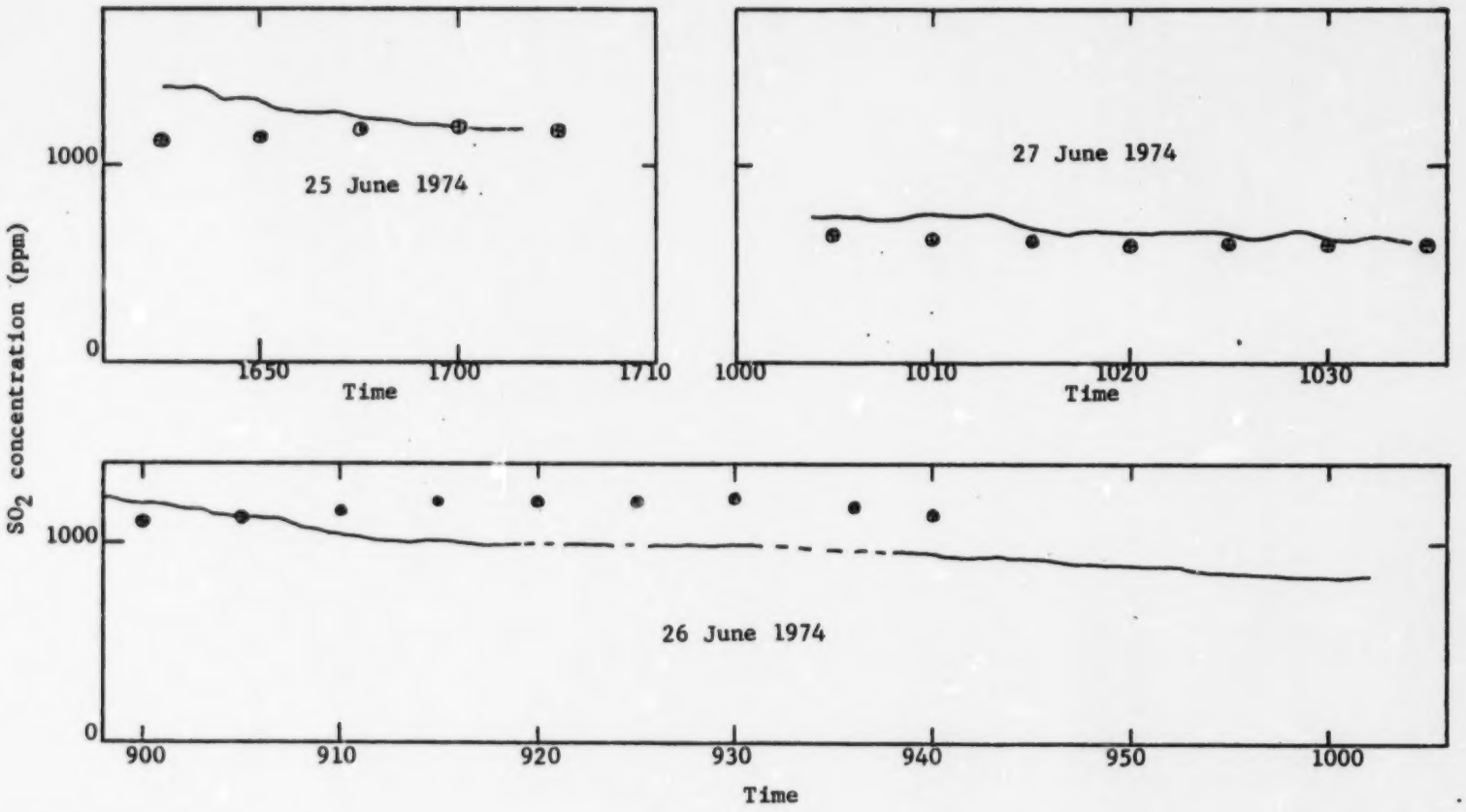

FIG. 26. Plots of SO_2 concentration vs time of day for 3 different days at Duke Power Co. in Charlotte, N.C. The time during zero adjustment and checking is represented by the dashed lined in the lower figure. The peak-to-peak noise was 120 ppm. The symbol ⊕ represents data obtained with the DuPont Model 460-1 analyzer.

SECTION 4

REFERENCES

1. Burch, D. E., and J. D. Pembrook. "Instrument to Monitor CH_4, CO, and CO_2 in Auto Exhaust." Prepared by Philco-Ford Corp. for EPA under Contract No. 68-02-0587. EPA Report No. 650/2-73-030, Oct. 1973.

2. Ludwig, C. B., Bartle, and M. Griggs. "Study of Air Pollutant Detection by Remote Sensors." Prepared for National Aeronautics and Space Administration under Contract NAS12-630 by Convair Division of General Dynamics. Report No. GDC-DBE68-011, Dec. 1968.

3. Bartle, E. R., S. Kaye, and E. A. Meckstrath. "An In-Situ Monitor for HCl and HF," AIAA Paper No. 71-1049, presented at the Joint Conference on Sensing of Environmental Pollutants, Palo Alto, Calif., Nov. 1971.

4. Goody, R. "Cross-Correlating Spectrometer," J. Opt. Soc. Am. 58, 900 (1968).

5. Advances in Environmental Science and Technology, John Wiley and Sons, Publishers, 1971. Edited by J. N. Pitts and R. Metcalf. Discussion on gas cells appears in a section "Spectroscopic Methods for Air Pollution Measurements," by P. L. Hanst.

6. Burch, D. E. "Adjustable Bandpass Filter Employing a Prism," Appl. Opt. 8, 649 (1969).

7. Decker, J. A., Jr. "Experimental Realization of the Multiplex Advantage with a Hadamard-Transform Spectrometer," Appl. Opt. 10, 510 (1971).

8. Abels, L. L., and J. H. Shaw. "Widths and Strengths of Vibration-Rotation Lines in the Fundamental Band of Nitric Oxide," J. Mol. Spectrosc. 20, 11 (1966).

9. Shaw, J. H. "Nitric Oxide Fundamental," J. Chem. Phys. 24, 399 (1956).

10. Burch, D. E., J. D. Pembrook, and D. A. Gryvnak. "Absorption and Emission by SO_2 between 1050 and 1400 cm^{-1} (9.5 - 7.1 μm ," prepared by Philco-Ford Corp. for EPA under Contract No. 68-02-0013. Philco-Ford Report No. U-4947, (ASTIA PB 203523), July 1971.

11. Benedict, W.S., R. Herman, G. E. Moore, and S. Silverman. "The Strengths, Widths, and Shapes of Lines in the Vibration-Rotation Bands of CO." Astrophys. J., 135, 227 (1962).

REFERENCES (Cont'd.)

12. Benedict, W. S., R. Herman, G. E. Moore, and S. Silverman. "The Strengths, Widths, and Shapes of Infrared Lines II. The HCl Fundamental." Can. J. Phys. 34, 850 (;956).

13. Meredith, R. E., and N. F. Kent. "Line Strength Calculations for the 0→1, 0→2, 0→3, and 1→2 Vibration-Rotation Bands of Hydrogen Fluoride." Prepared for the Advanced Res. Proj. Agency under Contract No. SD-91 by The University of Michigan. Report No. 4613-125-T, April 1966.

14. Herget, W. F., W. E. Deeds, N. M. Gailer, R. J. Lowell, and A. H. Nielsen. "Infrared Spectrum of Hydrogen Fluoride: Line Positions and Line Shapes. Part II. Treatment of Data and Results." J. Opt. Soc. Am. 52, 1113 (1962).

15. Goody, R. M., "Atmospheric Radiation", 1964, Oxford University Press.